ACS Electrochemistry

pubs.acs.org/electrochem
Review

From Pure to Seawater Electrolysis: Unveiling the Impact of Ionic Species and Contaminants on Electrocatalysis

Sahanaz Parvin, Emmanuel Aransiola, Sonakshi Saini, Matthew T. McDowell, Seunghoon Lee, Juliane Weber, Yiqing Wu, Yuanyuan Li, Chang Liu, Zili Wu, and Jonas Baltrusaitis*

Cite This: ACS Electrochem. 2026, 2, 43−67

ABSTRACT: Water electrolysis, including seawater splitting to produce hydrogen and oxygen, stands as a promising approach for the efficient storage of intermittent energy. However, the half-reactions of water splitting, the oxygen evolution reaction (OER) and hydrogen evolution reaction (HER), are known to be very sensitive toward the quality of water employed and are susceptible to contaminants originating from various sources, including the electrolyte or the electrodes. Those contaminants have a profound impact on the activity of these reactions of water splitting by modifying the electronic and physical structures of electrocatalysts as well as electrode−electrolyte interfaces. For seawater electrolysis, the unintentional presence of impurities, such as anions, cations, and organic compounds, affects the catalyst stability, selectivity, and activity. Despite the existence of numerous comprehensive reviews that delve into various aspects of catalysts and their structure−property relationships for several electrocatalytic reactions, the impact of contaminants has often been ignored. This critical review endeavors to address this issue by providing an overview of the diverse sources of contaminants influencing electrocatalytic water splitting and seawater splitting reactions, delineating the trends in electrochemical parameters and detailing different characterization methods for elucidating the physical and electronic changes of the electrode and electrolyte.

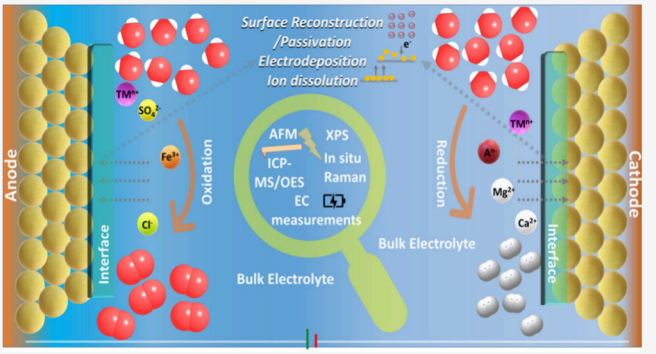

KEYWORDS: *electrocatalysis, hydrogen, contamination, seawater, OER, HER*

INTRODUCTION

The intensifying energy demand caused by rapid economic progress is an important challenge for the 21st century. The ongoing depletion of fossil fuels and the adverse environmental impact of nonrenewable energy sources underscore the critical need for the development of sustainable and renewable energy sources, such as hydrogen, solar energy, wind energy, and tidal energy.[1] Moreover, the increasing growth of artificial intelligence (AI) is leading to a sharp rise in electricity consumption largely from the data centers, which raises concerns about meeting the future energy demand.[2] Among these, hydrogen has particularly attracted significant attention due to its high gravimetric energy density (120 MJ kg^{-1}) and zero carbon emissions.[3] Although the electricity-driven hydrogen conversion efficiency is around 3 times lower than the heat-driven hydrogen conversion efficiency (steam methane reformation, steam−iron process), the latter is environmentally less benevolent due to the emission of greenhouse gases. Therefore, it is advisable to focus on eco-friendly approaches to produce hydrogen, such as electrocatalytic and photocatalytic water splitting, where abundant water is used as a feedstock.[4]

In a commercial electrolyzer, electrolysis of 45 kg of water is used to produce 5 kg of hydrogen.[5] This process involves the dissociation of water molecules into hydrogen and oxygen through an external electrical input. However, water electrolysis is inherently energy-intensive due to the sluggish four-electron water oxidation process at the anode (i.e., the oxygen evolution reaction, OER). The hydrogen evolution reaction (HER), a more energy-efficient two-electron process, takes place at the cathode.[6] To reduce the large activation energy barrier inherent in the uphill water splitting reaction, researchers are focusing on designing efficient catalysts. Although IrO_2 and RuO_2 are recognized as effective catalysts for the OER and Pt/C is the most widely used catalyst for the HER, their scarcity and high cost limit their practical applications.[7,8] Hence, the current scientific focus is on the design of materials based on cost-

Received: September 3, 2025
Revised: November 14, 2025
Accepted: November 21, 2025
Published: December 19, 2025

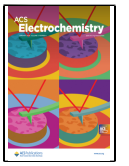

https://doi.org/10.1021/acselectrochem.5c00381
ACS Electrochem. 2026, 2, 43−67

Scheme 1. Schematic Illustration of the *Ex Situ* and *In Situ* Characterization Methods to Analyze Different Kinds of Contaminants in Various Catalysts for the Oxygen Evolution Reaction, the Hydrogen Evolution Reaction, and Seawater Splitting and Demonstrating Different Sources for Electrocatalytic Water Splitting.[a]

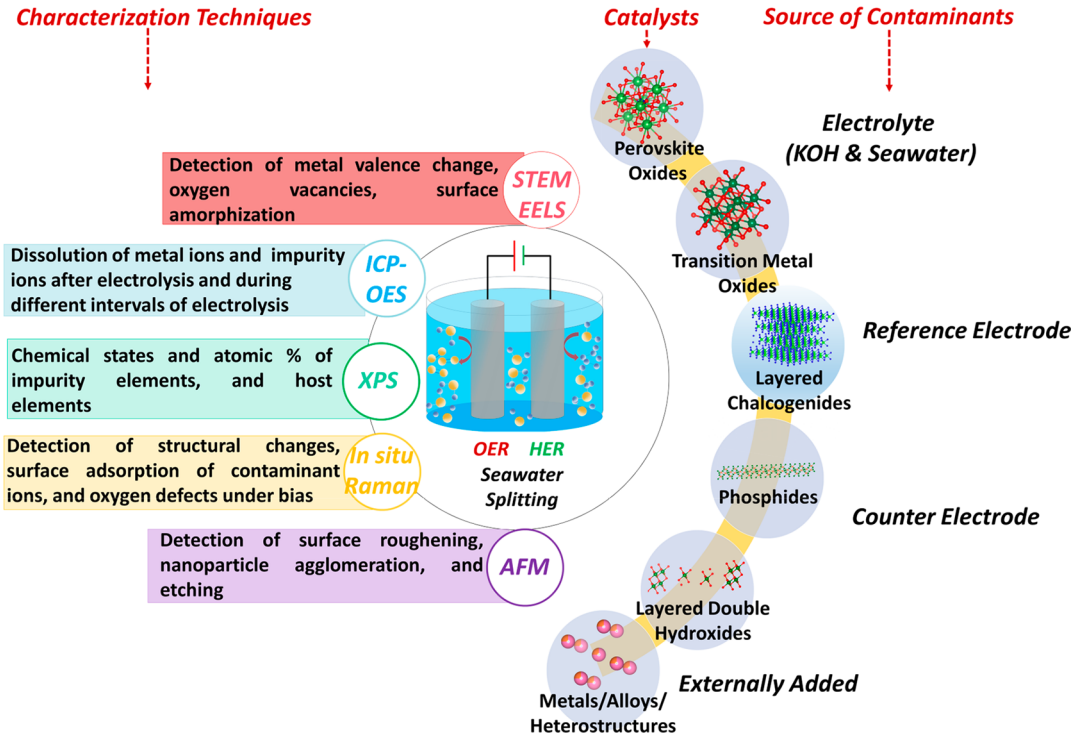

[a]STEM-EELS, ICP-OES, XPS, AFM, OER, and HER represent scanning transmission electron microscopy−electron energy loss spectroscopy, inductively coupled plasma optical emission spectroscopy, X-ray photoelectron spectroscopy, atomic force microscopy, oxygen evolution reaction, and hydrogen evolution reaction, respectively.

effective and earth-abundant transition-metal-based sulfides,[9] phosphides,[10] nitrides,[11] borides,[12] selenides,[13] oxides,[14] alloys, and hydroxides.[15] Various strategies are employed for enhancing the efficiency of the electrocatalysts by tuning the physical and electronic properties through doping,[16] introducing oxygen vacancies,[17] creating heterostructures or composite structures,[18] and tuning morphology.[19]

Despite significant efforts to design efficient electrocatalysts for hydrogen evolution, large-scale hydrogen production via the electrolysis of high-purity freshwater remains challenging, especially due to the scarcity of freshwater resources. This process not only depletes the limited freshwater resources but also necessitates costly water purification systems, thereby hindering its practical application.[20] Currently, more than 80% of the global population faces severe freshwater scarcity,[21] and large-scale water electrolysis further exacerbates the pressure on these vital resources. In this context, seawater electrolysis presents a promising solution, as seawater constitutes approximately 96.5% of the Earth's total water reserves.[22]

In the past few years, several pieces of literature have reported various probing molecules/ions (both cations and anions), intentionally added or unintentionally present as contaminants in the electrolyte, reactant, stemming from glassware, and the electrodes.[23−25] These literature reports show that the contaminants from various sources have a large impact on the electrocatalytic water splitting activity and stability due to the restructuring of active sites. Seawater is increasingly being considered as an alternative and practical feedstock due to the scarcity of freshwater resources; however, the presence of abundant impurities in seawater increases the complexity of electrochemical reactions, which is poorly understood. Accordingly, a comprehensive and systematic review of the meaningful work reported in the field is necessary. Herein we discuss the sources of contaminants and the types of contaminants (cations and anions) that influence the anodic and cathodic electrocatalytic water splitting reactions and the contaminants present during seawater splitting. Our review also covers the thermodynamics and fundamental parameters used in elecetrochemical water splitting and seawater splitting; characterization methods such as scanning transmission electron microscopy−electron energy loss spectroscopy (STEM-EELS), inductively coupled plasma optical emission spectroscopy (ICP-OES), inductively coupled plasma mass spectroscopy (ICP-MS), X-ray photoelectron spectroscopy (XPS), atomic force microscopy (AFM), which are used to analyze contaminant effects across a wide range of catalysts and ion exchange membranes; and strategies for mitigating these effects (Scheme 1).

This figure highlights the effects of contaminants originating from different sources based on the analysis and interpretation of the available published electrochemical data.

Finally, future perspectives are also highlighted in this review. Although there are prior literatures with a similar theme,[26−28] those reviews and perspectives primarily focus on specific aspects such as iron-mediated activation mechanisms, conventional freshwater systems, and generalized impurity effects on electrode kinetics. Our review uniquely synthesizes (i) a broad overview of both intentionally added and incidental species (cations and anions), (ii) contaminant sources including reference and counter electrodes, (iii) explicit discussion of

https://doi.org/10.1021/acselectrochem.5c00381
ACS Electrochem. 2026, 2, 43−67

seawater-specific challenges (cathode fouling, chlorine evolution reaction (ClER) side reaction trade-offs), and (iv) concrete, forward-looking recommendations (rational catalyst design, *operando* methods, dynamic electrode−electrolyte interface engineering, and spin and magnetism effects under realistic conditions during electrocatalysis) to guide future research and scale-up.

1. WATER ELECTROLYSIS

1.1. Thermodynamics and Kinetics. It is instructive to outline the fundamental definitions of thermodynamic and kinetic phenomena in water electrolysis and the associated definitions further used to describe the contaminant effects on the electrocatalysts. In water electrolysis, water is dissociated to form H_2 at the cathode and O_2 at the anode by applying electrical energy—these processes are known as the HER and OER, respectively.

The standard cell potential of water electrolysis (E°_{cell}) is described as the difference between the standard cathodic and anodic potentials, according to eqs 1−3):[29]

$$2H^+(aq) + 2e^- \rightarrow H_2(g) \quad E^\circ_{cathode} = 0\ V \tag{1}$$

$$2H_2O(l) \rightarrow O_2(g) + 4H^+(aq) + 4e^- \quad E^\circ_{anode} = 1.23\ V \tag{2}$$

$$E^\circ_{cell} = E^\circ_{cathode} - E^\circ_{anode} = -1.23\ V \quad \text{at } 25\ ^\circ C \text{ and pH } 0 \tag{3}$$

The half-cell potentials are denoted versus the reversible hydrogen electrode (RHE) at pH 0. Therefore, a cell voltage of 1.23 V must be applied to drive the reaction under standard conditions, although experimentally, an excess voltage is needed. From a thermodynamic perspective, water electrolysis is not spontaneous due to the positive Gibbs free energy (ΔG) of ~237.2 kJ/mol.

The excess applied voltage is described as the overpotential for electrochemical water splitting, which has four components, as specified in eq 4:

$$\eta_{total} = \eta_{HER} + \eta_{OER} + \eta_c + \eta_{iR} \tag{4}$$

where η_{HER} and η_{OER} are the overpotentials for the HER and OER, respectively, η_c is the concentration overpotential caused by the decrease in reactant concentration at the surface of the electrode relative to the bulk due to mass transport limitations, which can be minimized by stirring the electrolyte, and η_{iR} is the Ohmic voltage drop caused by the resistance of the aqueous electrolyte and the distance between the electrodes.[30,31] Both η_{HER} and η_{OER} can be minimized by fabricating an efficient catalyst over the electrode. Specifically, assuming Arrhenius behavior for the interfacial charge transfer kinetics, an exponential relationship between the overpotential (η_{HER} or η_{OER}) and the current density or rate (j) of the reaction is established, as shown in eq 5:[31]

$$j = j_0 \exp\left(\frac{\alpha n F}{RT}\eta\right) \tag{5}$$

where j_0 is the exchange current density, R is the gas constant, T is the absolute temperature, n is the number of electrons exchanged, and α is the fraction of the overpotential that reduces the energy barrier for reaction at the electrode−electrolyte interface (also known as the charge transfer coefficient).

1.2. Activity, Stability, and Selectivity Parameters of Catalysts. The electrochemical activity, stability, and selectivity of an electrocatalyst are governed by several electrochemical parameters, including the adsorption strength of hydrogen or oxygen molecules/intermediates on the catalytic sites, overpotential, mass loading of the catalyst, Tafel slope, turnover frequency (TOF), and Faradaic efficiency (FE). An efficient electrocatalyst should have long-term stability, high selectivity toward products, and efficient activity.

1.2.1. Adsorption Strength. The adsorption strengths of reactants, intermediates, and products on the catalyst surface are important descriptors for determining the catalytic activity and stability. Volcano plots are generally employed to establish the relationship between the exchange current density or overpotential and the adsorption free energy for different metals and various catalysts, respectively.[1,32,33] The rate of the HER largely depends on the hydrogen adsorption free energy (ΔG_H*) and hydrogen binding energy (HBE). If the adsorption is too weak, then the total reaction rate will be controlled by the adsorption step (Volmer step), whereas strong adsorption will cause the desorption step (Heyrovsky/Tafel step) to be the rate-determining step. According to the Sabatier principle, the adsorption and desorption should be optimal, neither too weak nor too strong, where $\Delta G_H \sim 0$. Following the relationship between ΔG_H* and the exchange current density (j_0), a volcano plot is established, which shows that Pt is expected to be the most active catalyst, having $\Delta G_H \sim 0$.[1]

Similarly, in the case of the OER, the activity is related to the oxygen adsorption free energy (ΔG_O). However, the single descriptor ΔG_O for the OER activity is incomplete because of the involvement of multiple intermediates (including OOH*, OH*, and O*). Moreover, the energy difference between the adsorption energies of OH* and OOH* has almost a constant value of 3.2 eV and is independent of potential in broad classes of metal oxide materials and metal surfaces.[34] As a result, a volcano trend between the OER activity and the two-descriptor difference $\Delta G_O - \Delta G_{OH}$ has been reported, and the optimal activity can be obtained by either weakening O binding or strengthening OH binding to the catalysts.[1] The optimization of binding between the intermediates and the catalyst surfaces can significantly improve the OER activity, although the OER activity cannot be improved beyond that of IrO_2.[34]

1.2.2. Overpotential. Both redox reactions associated with water electrolysis require potentials beyond the thermodynamically defined potentials of 1.23 V vs RHE for the OER and 0 V vs RHE for the HER. Beyond this thermodynamic potential, the excess potential needed to carry out a reaction at a specific rate is known as the overpotential.[35] In academic studies, the benchmark current density is chosen to be 10 mA cm^{-2} (this is the current density expected for a solar-to-fuels device with 10% solar-to-fuel conversion under 1 sun illumination). This value serves as a practical benchmark for evaluating the efficiency and feasibility of water-splitting systems in real-world solar-driven applications. Although industrial water-splitting processes typically operate at significantly higher current densities (e.g., 100−500 mA cm^{-2}), 10 mA cm^{-2} provides a useful starting point for screening and assessing catalyst materials before transitioning to large-scale implementation.[36,37] However, for catalysts having intense redox peaks due to metal oxidation, the overpotentials are considered at higher current densities (50−1000 mA cm^{-2}).[38] In addition to reporting overpotential at a specific current density, some studies on OER and HER catalysts also report the current density at a given overpotential. For example, j_{500} denotes the current density achieved at an overpotential of 500 mV.[39] The

https://doi.org/10.1021/acselectrochem.5c00381
ACS Electrochem. 2026, 2, 43−67

Scheme 2. Flowchart Showing the Steps Required to Calculate a Relatively Accurate TOF for Different Electrocatalytic Materials Used in Energy Conversion Electrocatalysis[a]

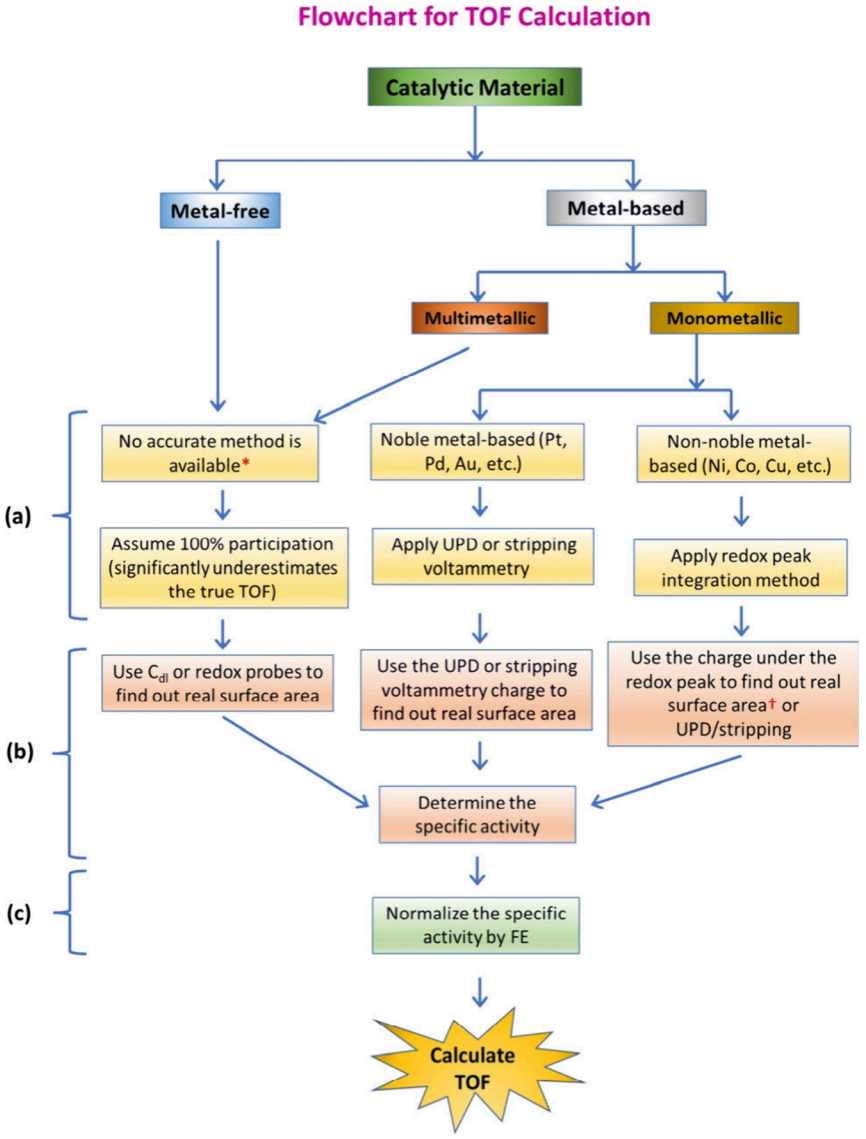

[a](a) The step determining the exact number of active sites participating in the catalysis. (b) The step excluding errors imparted by other ways of current normalization (with geometrical area, mass, etc.). (c) The step excluding errors for catalysts with FE < 100 %. Notes: *Electrochemical surface area obtained by dividing C_{dl} by C_s and other futuristic methods can be used only when lattice parameters are known. †Requires lattice parameters. Adapted from ref 42. CC BY 4.0.

geometric current density is significant for the engineering perspective, but it depends on several extrinsic parameters like mass loading, the accessible active sites, and the surface area.[40]

1.2.3. Tafel Slope and Exchange Current Density. In the case of low current and efficient stirring, the current is not controlled by mass diffusion; rather, it is regulated by the interfacial dynamics. According to previous studies, for these systems the current density (j) or rate of electrochemical reaction is related exponentially to the overpotential via eq 6:[41]

$$\eta = a + b \log j \tag{6}$$

where η is the overpotential, b is the Tafel slope, and a is the exchange current density.

1.2.4. Turnover Frequency (TOF) and Faradaic Efficiency (FE). The TOF is a measure of the efficiency of a catalyst in terms of the catalytically active sites, so it is considered a straightforward intrinsic activity indicator that can estimate how efficient a catalyst is for the reaction of interest. TOF is defined as the number of gas molecules evolved per unit time per active site of the catalyst[40] and is calculated using eq 7:

$$\mathrm{TOF} = \frac{iN_A}{Fn\Gamma} \tag{7}$$

where i is the current, N_A is the Avogadro constant, n is the number of electrons transferred in the electrochemical reaction, F is the Faraday constant, and Γ is the surface concentration of active sites. TOF is the basis for determining electrocatalytic efficiency, and a higher TOF means a higher intrinsic electrocatalytic efficiency. Although TOF is a straightforward intrinsic activity indicator, there are complications in determining the exact number of active sites participating in the catalysis,

https://doi.org/10.1021/acselectrochem.5c00381
ACS Electrochem. 2026, 2, 43−67

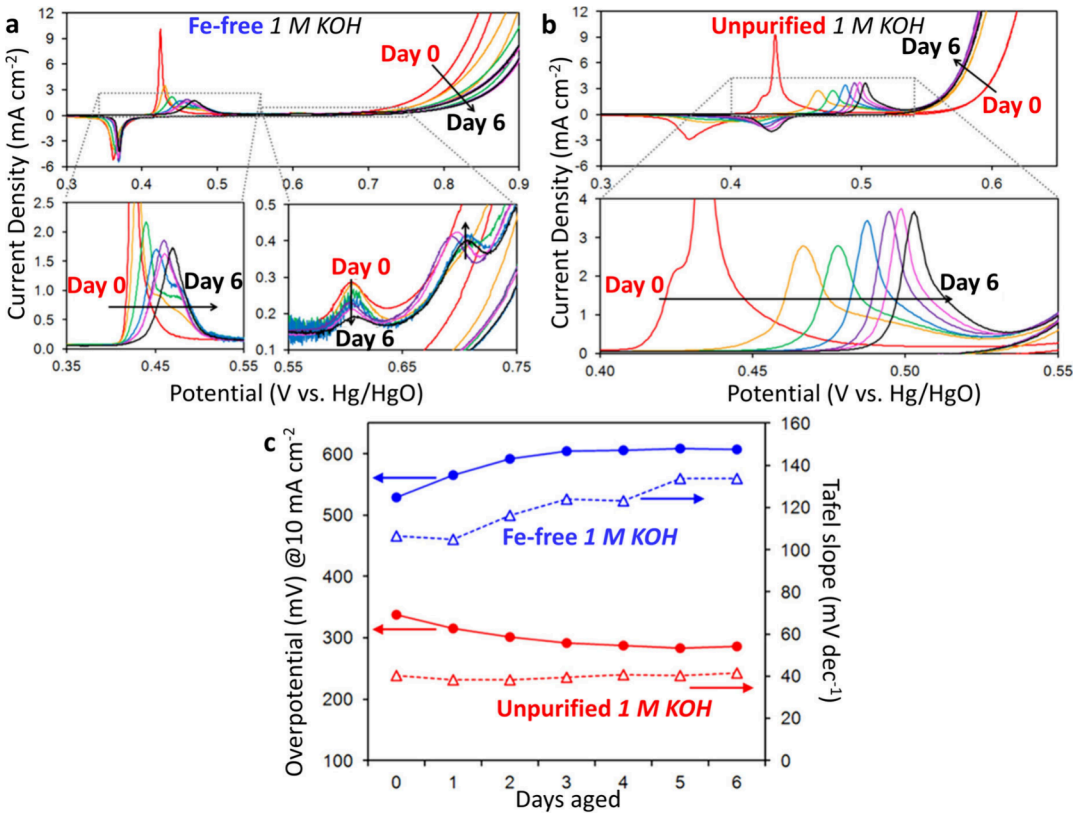

Figure 1. Cyclic voltammograms obtained for a $Ni(OH)_2$ film deposited on polished Au rotating disk electrodes (RDEs). Voltammograms were collected at 10 mV s^{-1} and 1600 rpm in (a) Fe-free and (b) unpurified 1 M KOH after each day of aging in either Fe-free or unpurified 1 M KOH, respectively. The oxygen evolution equilibrium potential is 0.306 V vs Hg/HgO in 1 M KOH. (c) Effect of aging on the overpotential at 10 mA cm^{-2} geometric current density (filled circles) and Tafel slope (open triangles) for $Ni(OH)_2$ films deposited on polished Au RDEs aged in Fe-free (blue) vs unpurified (red) 1 M KOH. Adapted from ref 58. Copyright 2015 American Chemical Society.

and TOF is often not properly reported.[42] The accurate method and process for calculating TOF is described in Scheme 2.[42]

The FE is defined as the molar quantity of the experimentally collected product relative to the amount that could be theoretically produced from the total charge passed (FE = $Q_{product}/Q_{total}$). The gas products are typically analyzed by gas chromatography (GC) at the outlet of the in-line electrochemical cell.

Higher FE means higher product selectivity, and the importance of reliable FE reporting and a standard method for measuring FE has also been addressed.[43]

1.2.5. Catalytic Stability. Catalyst stability is evaluated from performance retention either by performing long-term cycling in a fixed potential range with a fixed scan rate[44] or by keeping the electrode at a constant potential or current density for a particular time. If the working electrode is kept at a fixed potential, the stability measurement is typically named chronoamperometry, as it measures the change of current density with time,[45] whereas the measurement conducted at a fixed current density is known as chronopotentiometry.[46] For the cyclic stability measurement, a catalyst should show similar performance in a steady-state polarization measurement after a long number of cycling experiments conducted by cyclic voltammetry (CV).

2. INTERFERENCE OF IONIC CONTAMINANTS

2.1. Interference of Contaminants during the Oxygen Evolution Reaction (OER). *2.1.1. Effect of Cations.* The OER is an indispensable part of many energy storage and conversion systems, such as metal−air batteries,[47] solid oxide electrolysis cells,[48] CO_2 reduction reactions to valuable fuels,[49] and hydrogen fuel evolution from electrolysis of water.[50] Over the past few decades, researchers have focused on developing hybrid and advanced functional materials for OER, which have high activity and long-term durability.[51] IrO_2 and RuO_2 are among the most active catalysts for the OER reported to date. However, their scarcity and expensive nature limit their applications.[52] Hence, there is a strong interest in catalysts designed by engineering the first-row (3d) transition metals such as Ni, Co, and Fe via varying the d-band center of the cation site.[53−55] Previous literature also reports that doping of secondary transition metals in the catalysts can enhance OH^- adsorption, thus facilitating the formation of active species and consequently improving the OER activity.[56] Besides cation doping in the catalyst, the cations present in the electrolyte affect the reaction rate by tuning the electrical double layer (EDL) at the interface between the electrode and electrolyte. Kozawa observed that the addition of $Sr(ClO_4)_2$ increased the overpotential for OER on a Pt working electrode, whereas further addition of EDTA decreased the overpotential due to the complex formation between $Sr(ClO_4)_2$ and EDTA.[57] The increase in the overpotential for the three alkaline earth metals follows the order $Ca^{2+} > Sr^{2+} > Ba^{2+}$. Aside from Pt, other working electrodes such as Ni, Pd, NiO, Au, and graphite also exhibited an increase in overpotential upon the addition of $Sr(ClO_4)_2$, ranging from 15 to 90 mV depending on the electrode material. This was accompanied by a slight increase in the Tafel slope.

https://doi.org/10.1021/acselectrochem.5c00381
ACS Electrochem. 2026, 2, 43−67

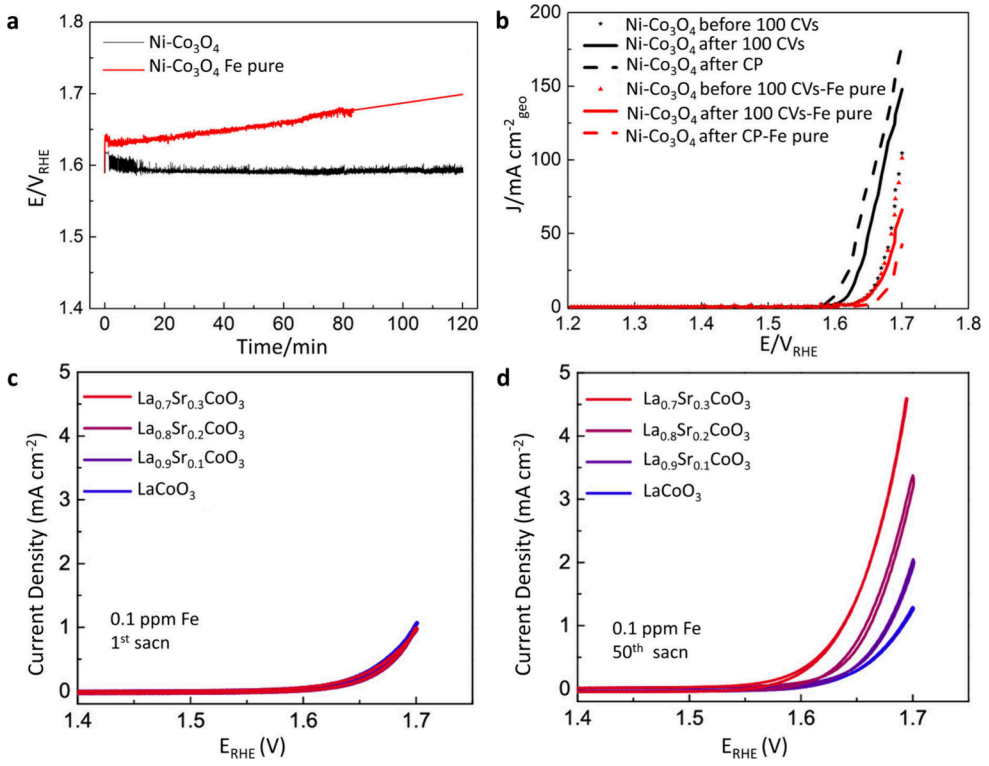

Figure 2. (a) Chronopotentiometry stress test profiles of the Ni−Co_3O_4 catalyst with and without Fe in solution at 10 mA cm^{-2} for 2 h. (b) Activity comparison of the Ni−Co_3O_4 catalyst between 1.2 and 1.7 V RHE at the 5 mV s^{-1} scan rate in Fe-contaminated (black) and Fe-pure (red) 1 M KOH. Adapted from ref 61. Copyright 2019 American Chemical Society. (c) First OER polarization curve for LSCO with 0, 10, 20, and 30% Sr content in A-sites and (d) after 50 potential cycles up to 1.7 V in 0.1 mol L^{-1} KOH deliberately containing 0.1 ppm Fe(aq). Adapted from ref 64. Copyright 2021 American Chemical Society.

Among all other transition metals, Ni has attracted significant attention for alkaline OER because of its high catalytic efficiency, low price, high elemental abundance, good mechanical properties, high corrosion resistance, good heat conduction, and high electrical conductivity.[59] The most active phase of Ni-based electrocatalysts is NiOOH, which contains Ni^{3+}. This phase is formed by the oxidative transformation of Ni-based materials at potentials near the onset of the OER.[60,61] According to the previous literature, the Fe^{3+} cation had the most profound impact on the electrocatalytic OER activity of Ni-based catalysts.[62] In $Ni_xFe_{1-x}OOH$, the contraction of the Fe−O bond optimizes the binding energy for the OER intermediates. There is a drastic decrease in current density after aging of the $Ni(OH)_2$ electrodes in Fe-free electrolytes, whereas dramatically opposite behavior is perceived in Fe-containing electrolytes (Figure 1a,b).[58] It has been observed that when an electrodeposited $Ni(OH)_2$ film was aged in purified 1 M KOH, the overpotential to achieve 10 mA cm^{-2} current density was increased by 76 mV after 3 days, whereas in unpurified 1 M KOH, the overpotential for aged films was only 280 mV after 5 days of aging.[58] The corresponding Tafel slope values also indicated the enhanced kinetics due to the aging in unpurified electrolytes, which was comparable with the kinetics of NiFeOOH catalysts reported in previous literature (Figure 1c).[58,63] Furthermore, the authors found that the TOF was lower initially, became maximized after 3−4 days of aging with Fe content of 11%, and then further decreased.[58] The initial decrease might be due to the sufficiently low Fe concentration to provide better activity or that Fe was not incorporated at the proper sites of the NiOOH lattice, and after achieving the maximum concentration, the TOF decreased due to the saturation of the active NiOOH phase and the generation of the less active Fe-rich phase.

The doping of other transition metals, such as Co and Mn, in Ni-based materials has also proven to be beneficial for activating Ni-based catalysts for OER.[65,66] Spanos *et al.* showed the improved activity of Ni−Co_3O_4 catalysts in Fe-contaminated electrolytes. Initially, in Fe-free and Fe-contaminated electrolytes the catalyst showed similar activities, but the activities largely deviated after 100 CV cycles and 2 h chronopotentiometry under the OER potential. In Fe-contaminated KOH, there was a initial increment in the OER activity, and then the catalyst was stable during 2 h chronopotentiometry, whereas in Fe-free KOH, deactivation of the catalyst was observed due to the corrosion of Ni and Co.[61] Accordingly, Fe contamination in the alkaline electrolyte not only activated the catalyst but also stabilized it by preventing its degradation (Figure 2a,b).[61]

Apart from the transition-metal-based oxides and oxyhydroxides, perovskite-type materials with the ABO_3 structure are the other class of materials that are observed to be very promising for OER. Here, the A site cations, which are generally alkali metal or rare earth metal cations, facilitate O_2 production from the lattice oxygen, and the B site cations (generally transition metal cations), trigger the oxidation of OH^- to O_2.[67,68] Lopes *et al.* reported the surface reconstruction dynamics of the perovskite oxides for OER due to the presence of contaminants in the alkaline electrolyte.[64] The authors demonstrated that the interaction of a few-nanometer-thick Co oxyhydroxide layer on the perovskite surface with trace-level Fe impurities creates a dynamically stable, surface-reconstructed active site for the OER. There was a dynamic equilibrium between the Fe dissolution and redeposition on the host Co

https://doi.org/10.1021/acselectrochem.5c00381
ACS Electrochem. 2026, 2, 43−67

oxyhydroxide lattice. The $La_xSr_{1-x}CoO_3$ perovskite oxide showed a noticeable enhancement in OER activity in the 50th CV scan upon the introduction of 0.1 ppm Fe in the electrolyte, which increased with an increase in Sr doping. However, all the perovskites showed similar OER activity in the first scan under similar electrochemical conditions (Figure 2c,d).[64] Here, the strategy for designing active and stable catalysts for OER (e.g. Fe_x-BOH_y@ABO_3) was manifested, where the choice of A-site cations, such as La, Sr, or Ba, has been shown to promote O_2 evolution through an indirect route where surface oxygen atoms originating from the crystal lattice participate in forming molecular oxygen and manipulating the B-site metals affects the H_2O/OH^- oxidation mechanism.[64] The perovskites without any "A" or "B" site doping also exhibited a change in the anodic redox peak as well as electrocatalytic OER activity upon introduction of Fe^{3+} ions in the electrolyte.

Twight *et al.* reported the effect of Fe introduction in a purified KOH electrolyte for undoped $LaNiO_3$ particles, $LaNiO_3$ epitaxial films, and an analogous Ruddlesden−Popper phase, La_2NiO_4 catalysts.[24] The catalytic current, normalized to the integrated charge associated with redox-active nickel during the Fe spike experiments, indicates that the redox-active species exhibit comparable OER activity characteristics despite the differing structures of the host materials $LaNiO_3$ and La_2NiO_4. However, La_2NiO_4 demonstrates a greater propensity for the accumulation of redox-active nickel compared to $LaNiO_3$, highlighting the importance of Ni−O termination in the development of these surface species.[24] For both crystal phases, Fe incorporation increased the OER activity, and the prolonged cycling in the presence of Fe further increased the OER activity.

Although most of the literature reported the impact of intentional or unintentional addition of Fe in a variety of catalysts, Naderi *et al.* recently reported the effect of all the d-block transition metals, such as Fe, Co, V, Cr, Mn, Cu, and Zn, as impurity metal cations on the surface of $Ni(OH)_2$ for OER.[69] Surprisingly, except Fe, other cations had a negligible effect on the OER activity of α-$Ni(OH)_2$, whereas by the addition of Fe in unpurified KOH, there was a decrease of the OER overpotential by 138 mV due to the formation of an active Ni−Fe-based catalyst. The authors showed that Fe preserved the actual structure of α-$Ni(OH)_2$ by preventing further oxidation of Ni and increased the rate of charge transfer and the surface area.[69]

Pham *et al.* observed that Fe was not deposited on bare glassy carbon (GC) electrodes by CV or chronopotentiometry during OER; it could only be incorporated in the Co host lattice by substituting Co with Fe.[70] They conducted consecutive CV cycles in the presence of Fe and Co ions in KOH electrolyte. After the 10th CV cycle, Fe did not deposit on the GC electrode, but Co deposited anodically, forming a mixture of crystalline Co_3O_4, crystalline CoO, and amorphous CoO_x, which increased the OER activity of GC with an overpotential of 395 mV at a current density of 10 mA cm^{-2}. The Co-deposited GC anode showed promising OER activity in KOH with added 0.2 mM Fe electrolyte, where the deposited Fe^{3+} in the Co host lattice replaced Co^{3+} and formed an OER-active Fe-doped Co mixed oxide catalyst on GC, exhibiting an improved overpotential of 319 mV at 10 mA cm^{-2}.[70]

The rate of the OER and the surface coverage of adsorbents during the OER are found to be critically dependent on pH. Typically, electrocatalytic reactions are conducted under extreme pH conditions with high concentrations of OH^- or H^+ ions to mitigate the impact of mass diffusion limitations. There is a lack of studies examining the combined effects of contaminants and pH on OER. The influence of impurities on OER activity is significant, particularly when decreasing the pH to 13 (0.1 M KOH) from 14 (1 M KOH). In 0.1 M KOH, without any contamination from iron, the aging of $Ni(OH)_2$ displayed distinct structural changes (redox transformation) compared to when the electrolyte contains Fe.[58] Specifically, when the electrode film was aged in unpurified electrolyte (containing Fe), it led to the transformation of nickel hydroxide to NiFe-LDH (layered double hydroxide). Furthermore, this transformation hindered the usual Bode scheme progression of structural transformations to β-NiOOH and then to γ-NiOOH under an anodic potential.

Existing literature suggests that the perovskite oxides generally exhibit a noteworthy correlation between OER activity and pH.[64] No change in OER activity was observed in both purified KOH and KOH with added 1 ppm Fe for 30% Sr-doped $LaCoO_3$ (LSCO-30), and $LaCoO_3$ (LSCO-0) catalysts as the pH was reduced from 14 (1 M KOH) to 13 (0.1 M KOH) to 12 (0.01 M KOH).[64] However, in commercial unpurified KOH with an uncontrolled and unknown amount of Fe, there was a decrease in the OER activity with a decrease in pH. This reduction in activity was mainly due to a 10- and 100-fold dilution of the Fe concentration in the pH 13 and 12 solutions, respectively, and the effect was particularly more prominent in the LSCO-30 perovskite than in the undoped perovskite (LSCO-0) due to the faster surface evolution in the former catalyst.[64] These results further demonstrated that the OER kinetics and surface transformations were highly pH-dependent, with Fe contamination significantly impacting catalyst behavior.[58,64]

While numerous studies have highlighted the beneficial effects of Fe^{3+} ions in electrolytes for electrochemical water oxidation, Zhou *et al.* investigated the influence of the presence of a low concentration (5 ppm) of transition metal ions (Ni^{2+}, Fe^{3+}, Fe^{2+}, Co^{2+}, Mn^{2+}, Zn^{2+}, Ce^{3+}, and Al^{3+}) on the current density for a bare carbon paper (CP) electrode during electro-oxidation of water in 0.1 M KOH.[23] Among them, Co^{2+} exhibited the most pronounced effect, increasing the current at 1.7 V by a factor of 57. Additionally, electrochemical impedance spectroscopy (EIS) measurements revealed a significant reduction in the charge transfer resistance of the CP electrode, decreasing from 886.6 to 19.1 Ω in the presence of 5 ppm Co^{2+} in the electrolyte. However, the observed improvements in electrochemical performance were influenced by several key factors, including the pH of the electrolyte, the number of CV cycles, and the surface properties of the electrode.[23]

2.1.2. Effect of Anions. Like cations, the decoration of anions of the electrocatalysts also seemed to have a great effect on the electrocatalytic OER activity. The electronic structure of catalysts, especially metal hydroxides, was found to be tuned by the ornamentation with anions through the change in the interlayer distance and ease of transformation from metal hydroxide to oxyhydroxide.[71] Moreover, for metal basic salt catalysts, there is an "anion effect", where these catalysts performed better for the OER than their hydroxide counterparts. Systematic investigations on basic cobalt salts with F^-, Cl^-, or CO_3^{2-} anions revealed an OER activity trend as $Co(OH)(CO_3)_{0.5}$ > $Co_2(OH)_3Cl$ > $Co(OH)F$ > $Co(OH)_2$ which was attributed to the presence of a maximum number of active Co^{4+} sites in $Co(OH)(CO_3)_{0.5}$ due to the faster leaching of CO_3^{2-} from the lattice, compared to other anions.[72] Although there is literature on the anion-based modification of catalysts for OER,[73,74] very few reports on the effect of electrolytic anion on

https://doi.org/10.1021/acselectrochem.5c00381
ACS Electrochem. 2026, 2, 43−67

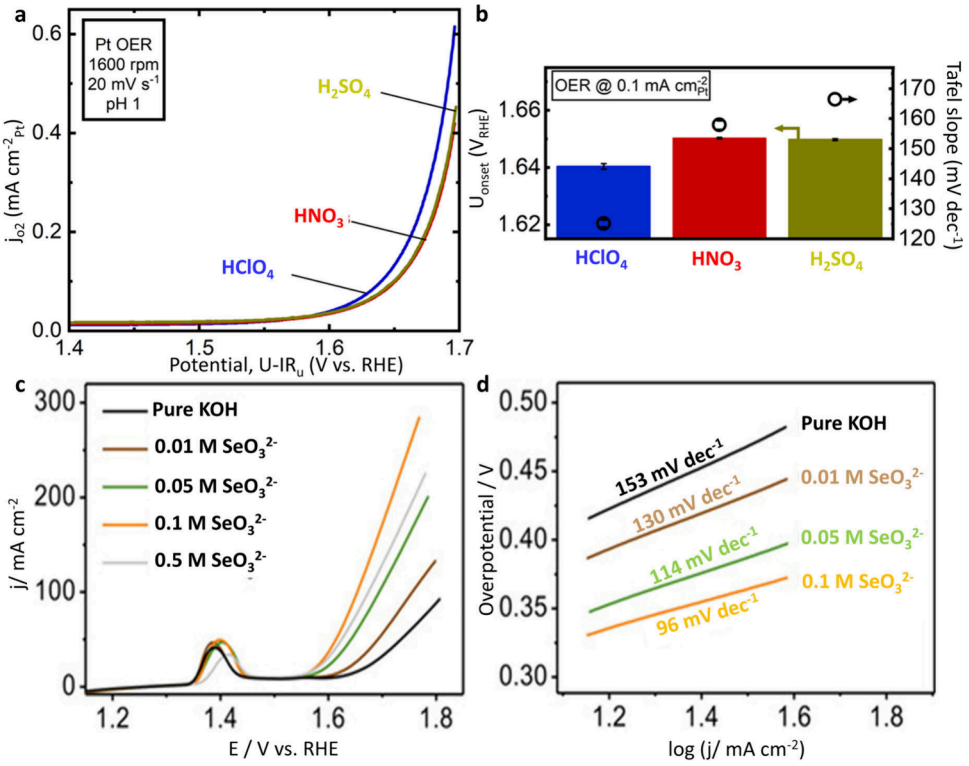

Figure 3. (a) Representative second-cycle-averaged oxygen evolution reaction (OER) RDE CV of the Pt disk in $HClO_4$, HNO_3, and H_2SO_4 at pH 1. The OER trend is consistent as a function of cycle. (b) Average OER onset potential (bars, left *y* axis) ±0.1 mA cm^{-2} Pt for all three acids and average Tafel slope (circles, right *y* axis) in the low current density region. Adapted from ref 75. CC BY 4.0. (c) OER activity comparison and (d) Tafel slopes of $Ni(OH)_2$ in 1 M KOH with different concentrations of SeO_3^{2-}. Adapted with permission from ref 39. Copyright 2020 Wiley-VCH.

Table 1. Summary of the Effect of Impurities on the Electrochemical Oxygen Evolution Reaction

catalyst	impurity	electrolyte	key results	ref
$Ni(OH)_2$	Fe	1 M KOH	OER activity increased due to formation of NiFe-LDH	58
$Ni–Co_3O_4$	Fe	1 M KOH	Significant improvement in OER activity due to activation of catalysts and prevention of catalyst degradation with lesser corrosion of Ni and Co	61
$La_{1-x}Sr_xCoO_3$	Fe	0.1 M KOH	Improvement in OER activity due to formation of dynamically stable active site	64
$Ni(OH)_2$	V, Cr, Mn, Fe, Co, Cu, Zn	1 M KOH	Maximum improvement in OER activity in the presence of Fe (decreases the overpotential up to 138 mV at a current density of 10 mA cm^{-2}), and then Co; decrease in OER activity in the presence of V, Mn, Cr, Cu, and Zn	69
			The electronic interaction between Ni and Fe prevents further oxidation of Ni(II)	
$LaNiO_3$, La_2NiO_4	Fe	1 M KOH	Increase in OER activity due to formation of $NiFeO_xH_y$ catalysts	24

OER were present in the literature. Pt is commonly used as a model catalyst to investigate the anion effect for the OER. When CV cycling was performed with a Pt disk as a working electrode in different electrolytes like $HClO_4$, HNO_3, and H_2SO_4, the measured OER onset potentials at +0.1 mA cm^{-2} Pt in $HClO_4$, HNO_3, and H_2SO_4 were observed as 1.64, 1.65, and 1.65 V vs RHE, respectively. Although this suggested similar behavior for OER at a particular current density, the lower Tafel slope in $HClO_4$ compared to HNO_3 and H_2SO_4 demonstrated changes in the adsorbates, rate-limiting steps, and mechanisms among $HClO_4$, HNO_3, and H_2SO_4 (Figure 3a,b).[75]

To elucidate these trends in the OER activity, the non-Faradaic charge passed at the electrode before the onset potential of the OER was calculated, which showed lesser anion adsorption in $HClO_4$ compared to HNO_3 and H_2SO_4, resulting in more active sites available for the OER in the $HClO_4$ electrolyte. Further calculations on the Pt (111) surface also demonstrated weaker anion adsorption in $HClO_4$ electrolyte, corroborating the previous data.[75] The chalcogens have shown a strong tendency to leach in the electrolyte during OER under oxidative bias.[76] Surface-absorbed selenates (the oxidized form of transition-metal-based selenides) have an important effect on the OER activity. This estimation was further verified by the intentional addition of SeO_3^{2-} into 1 M KOH using the $Ni(OH)_2$ catalyst, which exhibited an abrupt improvement of the OER activity. For an optimized concentration of SeO_3^{2-} (0.1 M), j_{500} increased from 47 to 221 mA cm^{-2} along with improved charge transfer kinetics (Figure 3c,d).[39] The surface-adsorbed selenates enhanced the OER activity by reducing the free energy of adsorption of intermediates as well as shifting the d-band center of NiOOH closer to the Fermi level.[39] The universality of the effect of SeO_3^{2-} was proved by the similar improvement in the OER activity for $Co(OH)_2$ and $Cu(OH)_2$ catalysts. Moreover, with the optimal addition of 0.1 M SO_4^{2-}, j_{500} of $Ni(OH)_2$ was also improved from 44 to 105 mA cm^{-2}, leading to the conclusion that surface-adsorbed SO_4^{2-} also showed

https://doi.org/10.1021/acselectrochem.5c00381
ACS Electrochem. 2026, 2, 43−67

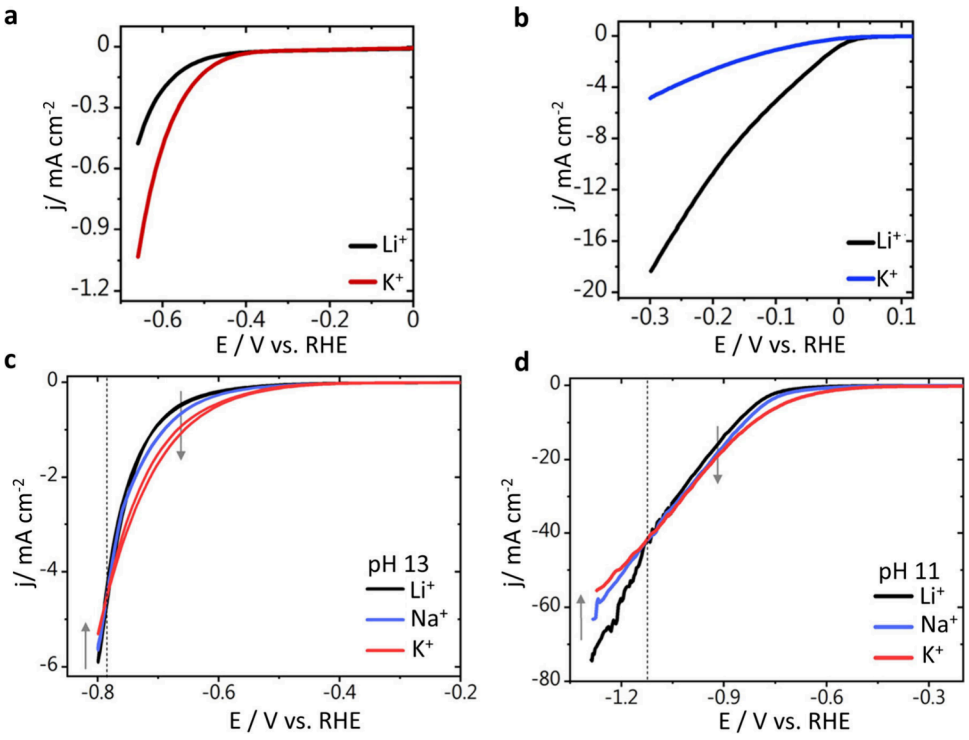

Figure 4. (a, b) Hydrogen evolution on stationary electrodes (a) gold and (b) platinum in alkaline media (0.1 M MOH, pH 13). (c, d) Hydrogen evolution cyclic voltammetry on a stationary gold electrode at (c) pH 13 and (d) pH 11 recorded in 0.1 M MOH and 0.001 M MOH (M = Li^+, Na^+, or K^+) at 50 mV s^{-1}. The dotted gray lines indicate the potential at which the CVs cross, and the arrows point in the direction from the strongly to the weakly hydrated metal cation species. Adapted from ref 77. CC BY-NC-ND 4.0.

improvement of OER activity by promoting the adsorption of the OER intermediates.[39]

2.1.3. Trends Observed Due to the Impurity Effect on OER Activity. The influence of different cations in purified KOH and the unintentional presence of Fe^{3+} in unpurified KOH on the OER activity of transition metal catalysts were discussed in previous scientific literature (Table 1).[24,58,61,64,69] In this context, transition-metal-based oxide, hydroxide, and perovskite oxide catalysts have been widely employed for investigating the OER activity. The inadvertent presence of Fe in KOH contributes to the formation of Fe-based multimetal oxyhydroxides on the surface of the catalysts, which were found to have remarkable catalytic activity for the OER. Consequently, most of these catalysts exhibit corrosion and a decline in the OER activity after a durability test conducted in purified KOH. This degradation is mainly attributed to the leaching of metals from the surface of the catalysts. However, when exposed to unpurified KOH enriched with Fe impurities, these catalysts exhibited a gradual increase in the catalytic OER activity.[58] Iron was identified as the dynamic active site for the OER in the multicomponent interface formed because of consecutive cycling or aging under the anodic potential. It is noteworthy that the observed trend in OER activity in the unpurified electrolyte was contingent upon several factors, including the dissolution of metals, the composition of the catalyst material, the electronic structure of the catalyst, and the pH of the electrolyte.[58,64]

Although unintentional anion contamination is not prominent for OER, there have been a few studies reporting on varying electrolytes with different anions, deliberate addition of anions in the electrolyte, and their effect on OER activity.[39,75] Depending on the free energy of adsorption of the anions on the surface of the electrocatalysts, the OER activity and the corresponding electrochemical parameters were found to vary.[39]

Moreover, the intentional addition of different d-block transition metals was also tested in an alkaline electrolyte, and Co^{2+} was observed to exhibit a pronounced enhancement in the OER activity on a bare CP electrode.[23]

To elucidate the impact of contaminants on the OER activity, several analytical techniques have been employed. These techniques include EELS,[64] XPS,[62] ICP-OES,[58] and electrochemical measurements.[58,23] Through the careful application of these advanced spectroscopic, electrochemical, and analytical methods, researchers have gained valuable insights into the intricate interplay among catalyst composition, impurities, and the OER activity in unpurified electrolyte solutions. While most of the literature focuses on the effects of cations in the electrolyte during the OER, studies addressing the influence of anionic contamination remain relatively scarce. The impact of anions on the performance of the OER is primarily governed by their adsorption strength and the specific nature of the adsorbed anions. These factors influence the free energy of adsorption of key intermediates in the OER pathway, thereby modulating the overall activity of the reaction.[39,75]

2.2. Interference of Contaminants during the Hydrogen Evolution Reaction (HER). *2.2.1. Effect of Cations.* Cations present in the electrolyte can directly affect the mechanistic aspects of the HER as well as the catalyst efficiency and selectivity. Different metal electrodes have been found to show varying effects in the presence of cations in the electrolyte.[77] From the Sabatier volcano plot (hydrogen binding energy vs logarithm of the exchange current density),[1,33] it was observed that the hydrogen binding energy is stronger on the surface of Pt and Ir compared to Ag and Au surfaces. Due to this

https://doi.org/10.1021/acselectrochem.5c00381
ACS Electrochem. 2026, 2, 43−67

Table 2. Summary of the Effect of Impurities on the Electrochemical Hydrogen Evolution Reaction

catalysts	impurity	electrolyte/reaction conditions	key results	ref
Pt-coated Ni	Cu Fe Cr R−NH_2 R−SH Hg	33% NaOH, 90 °C	No deactivation in the presence of Cu For other impurities, deactivation was observed within 10 to 100 h	82
Cu RDE	Fe	0.1 M NaOH and 0.1 M CsOH (unpurified)	A greater increase in current density was observed in CsOH than in NaOH	85
Au Pt	Cu	0.5 M H_2SO_4 + $CuSO_4$ (1 μM, 1 mM, 10 mM, 50 mM)	Decrease of current density with increasing $CuSO_4$ concentration for Pt and Au in CV analysis due to poisoning effect	81

behavior, the HER activities of these metal surfaces in the presence of different cations were found to vary. The metals with weak hydrogen binding exhibited the maximum HER activity in the electrolyte containing cations of a smaller size and greater hydration energy (and *vice versa*). These results confirm decreasing HER activity for Au and Ag and increasing HER activity for Pt and Ir with increasing hydration energy of the alkali metal cation (Li^+ > Na^+ > K^+ > Rb^+ > Cs^+). This phenomenon might be attributed to the change in the H-binding energy of the electrodes resulting from the interaction between the cations near the active site on the electrodes and the intermediates on the electrode surface.[78]

In agreement with the previous results, Monteiro *et al.* also observed a similar trend at lower alkalinity (0.1 M MOH), with the highest HER activities for the Au and Pt surfaces being in KOH and LiOH electrolytes, respectively (Figure 4a,b).[77] In contrast, this HER activity exhibited an inverse trend on the Au electrode at higher overpotentials, where the current density was found to be higher in LiOH, suggesting an increase in the local alkalinity at high overpotentials and a consequent increase in the near-surface cation concentration. Overall, weakly hydrated cations were found to be detrimental to water reduction at a more alkaline pH.[77] This was due to the pronounced effect of cation accumulation at the outer Helmholtz plane (OHP) with a lower hydration energy. When the pH was decreased from 13 to 11, this detrimental effect of HER activity in KOH was found to occur at a more negative potential compared to the electrolyte with a higher pH, since a more negative potential was required to acquire sufficient local alkalinity (Figure 4c,d).[77]

Pt has often been identified as the best HER catalyst due to its optimal hydrogen binding energy.[79] A variety of studies have investigated the poisoning effects of cations on platinum-based electrocatalysts for HER. Kötz and Stucki observed the poisoning effects on platinum and ruthenium dioxide in acidic media for a variety of metal cations. Copper and silver were found to poison platinum because their positive reduction potential was higher than that required for hydrogen evolution, which caused electrodeposition of the metals.[80] Other metal ions such as lead, tin, cadmium, and molybdenum were also found to poison platinum despite having lower reduction potentials, since underpotential deposition (UPD) can occur in the HER regime.[80] It was postulated that the electrocatalyst materials such as ruthenium dioxide might avoid this UPD poisoning effect since UPD was less prevalent on oxides and semiconductors, thereby making ruthenium dioxide a more suitable catalyst for HER in the presence of metal ion impurities. In a 1 N H_2SO_4 electrolyte, metallic Pt and semiconductor RuO_2 were observed to behave differently in the presence of Cu^{2+} and Cd^{2+} ions, which was due to the suppression of UPD in the case of RuO_2. The HER activity of Pt in the presence of both Cu^{2+} and Cd^{2+} ions decreased due to the deposition of the corresponding metals, whereas for RuO_2 it remained unchanged due to the suppression of UPD. For Cd^{2+} ions, the reversible deposition potential of Cd^{2+}/Cd was found to be cathodic to the hydrogen evolution potential, making the bulk deposition of Cd unfavorable. However, the deposition of the first monolayer of Cd was possible.

As another example, Cu deposition on the Pt surface takes place in parallel in the HER region, increasing the HER overpotential on Pt.[81] In the case of Cu deposition on Pt, the interaction between the adsorbate and the electrode was significantly stronger than the adsorbate−adsorbate interaction. This effect inhibited cluster growth, allowing only a monolayer of adsorbate to deposit, which was sufficient to poison the substrate. Conversely, Cu deposition on RuO_2 followed a distinct growth mechanism that promoted cluster formation without adversely affecting the HER activity.[80]

Generally, chlor-alkali membrane cell technology uses cathode catalysts with low hydrogen evolution overpotential.[82] A deactivation study of a Ni-based cathode was conducted by analyzing the increase in overpotential with time. For both efficient (catalytically active for HER) and nonefficient (having low catalytic activity for HER) electrodes, after a few hundred hours of electrocatalysis in the presence of Fe impurity, only Cu showed no noticeable effect on the HER activity due to the insufficient deposition in the form of a thin, porous structure.[82]

Another catalyst of interest for studying the effect of metal ions on electrochemical reduction reactions is copper, which is commonly used for the CO_2 electroreduction reaction (CO_2RR).[83,84] Li *et al.* found that trace quantities of iron in hydroxide salts dramatically increased the HER activity on Cu at higher pH values (~13). The kinetics of iron deposition on Cu was found to decrease with decreasing pH.[85]

2.2.2. Trends Observed Due to the Impurity Effect on HER Activity. In the case of HER, the modulation of activity was found mostly for different cations in alkaline electrolytes and with the addition of cationic impurities in acidic electrolytes (Table 2).[81,82,85] Depending on the hydrogen binding energy strength on the surface of the metal catalyst, the interaction in the EDL was varied as a function of the hydration energy of the cations in the alkaline electrolyte.[77,78] Moreover, in acidic electrolytes, depending on the reduction potential and value of the underpotential deposition of the impurity cations, the extent of degradation on the metal and semiconductor electrocatalyst varied.[80]

2.3. Effect of Inherent Ionic Impurities on Seawater Splitting. Many transition-metal-based catalysts have been reported for seawater splitting, such as VS_2@V_2C,[86] CoMoC/MXene/NC,[87] NiCoP/NF,[88] NiMoN,[89] $CoFe_2O_4$,[90] and CoFe-LDH.[91] However, one of the biggest challenges in seawater

https://doi.org/10.1021/acselectrochem.5c00381
ACS Electrochem. 2026, 2, 43−67

splitting is the interference by the many ions and other impurities in seawater, which decreases the overall splitting efficiency.[21] It is important to clarify that the major ionic constituents in seawater, such as Na^+, Mg^{2+}, Ca^{2+}, K^+, and Cl^-, are inherent species rather than the typical "contaminants". However, the term "contaminants" is used in the other sections of this review in a broader electrochemical context to describe any species, whether naturally present or externally introduced intentionally, that may interfere with the desired HER or OER and influence the catalytic activity and stability. Seawater is a highly complex electrolyte where these inherent ions, along with trace inorganic and organic species, can significantly modulate the local pH, ion transport, and chemistry at the electrode–electrolyte interface. Therefore, understanding these interactions is crucial for designing future catalysts with optimized seawater electrolysis efficiency.

The elemental composition of seawater is shown in Table 3, indicating the abundance of a wide variety of ions (potentially even in the cleaned feed of the electrolyzer).[92] For seawater splitting at scale, researchers have also used different concentrations of NaCl in the electrolyte to mimic natural seawater.[93] In the following section, a comprehensive discussion of the effect of cationic and anionic contaminants on seawater splitting is elaborated.

Table 3. Elemental Composition of Seawater[92]

element	concentration (mg/L)
Na^+	10,800
Mg^{2+}	1300
Cl^-	19,400
Ca^{2+}	400
K^+	400
SO_4^{2-}	2700
Br^-	70
F^-	1
HCO_3^-	100
CO_3^{2-}	10
Sr^{2+}	10
$B(OH)_3/B(OH)_4^-$	30
others	21–22

2.3.1. Effect of Cations. The cations that are naturally present in the seawater are the major hindrance to HER at the cathode during seawater splitting.[94] The most dominant dissolved cations in seawater are Na^+, Mg^{2+}, Ca^{2+}, and K^+.[20,95] These dissolved cations interact with the electrodes and catalysts to form inactive complexes, which affect the overall efficiency of water reduction, causing accelerated degradation of the electrocatalyst. H_2 formation at the cathode causes depletion of H^+ in the vicinity of the cathode, whereas OH^- depletion occurs at the anode. The depletion of H^+ and OH^- leads to changes in the pH.[95] When H^+ ions are depleted, the pH of the solution increases, whereas the pH decreases for OH^- depletion at the anode.[95] The rise in pH causes Ca^{2+} and Mg^{2+} ions in seawater to precipitate out as insoluble $Ca(OH)_2$ and $Mg(OH)_2$, a process commonly termed cathode fouling. These precipitates increase the HER overpotential by blocking the active sites available for electrochemical reactions.[96] Kirk and Ledas reported the tendency of an increase in pH from 6 to approximately 8–9 at the electrode surface during synthetic seawater electrolysis at 20 °C, and the cation composition of the precipitate was predominantly Mg^{2+} (approximately 95%) and Ca^{2+} (approximately 6%), causing electrocatalyst deactivation.[96] However, with an increase in the pH due to the long-term electrolysis, the precipitate predominantly contained calcium hydroxide and carbonates.[96]

Different strategies have been employed to address the problem of cathode fouling and precipitation of insoluble calcium and magnesium hydroxides. The ability to resist the effects of ions like Mg^{2+} and Ca^{2+} during seawater splitting is known as anti-position.[97] For example, increasing the valence state of transition metal ions was able to boost the HER activity in seawater.[98] The incorporation of oversaturated nitrogen atoms in 2D Mo_5N_6 attuned the electronic properties of Mo to conduct efficient HER in natural seawater.[98] The precipitation of alkaline earth metal-based hydroxides during seawater splitting was greatly affected by the local environment and pH. The introduction of Lewis acids, such as Cr_2O_3, over transition metal oxides mitigated precipitation (inhibition of precipitation of insoluble deposits at the electrode surface) of the Mg^{2+}- and Ca^{2+}-based hydroxides. Due to its Lewis acidic nature, Cr_2O_3 attracted the OH^- near the electrode surface, which not only increased the pH on the electrode surface, benefiting the HER, but also restricted the OH^- in the EDL, hindering the precipitation of Mg^{2+} and Ca^{2+} hydroxides in the bulk solution.[99]

2.3.2. Effect of Anions. Seawater contains a large amount of electrochemically active anions, predominantly Cl^- anions, that can interfere with the OER at the anode during electrolysis. When considering all the anions and the standard redox potentials of relevant species, it was found that the ClER could compete with the OER at the anode during seawater electrolysis because they have the same potential window. The ClER is a two-electron process with a standard electrode potential of 1.36 V vs SHE. At pH 0, $\eta_{ClER} > 0.10$ V and $\eta_{OER} > 0.23$ V are the typical overpotentials at which the ClER and OER are studied under industrial conditions. Under these conditions, the activities of the ClER and OER are governed by the OCl adsorbate and OOH adsorbate, respectively, and consequently, these determine the selectivity ratio of ClER and OER.[100]

Moreover, the selectivity strongly depends on the pH and Cl^- concentration.[101,102] Sohrabnejad-Eskan *et al.* investigated the effect of pH on the RuO_2 surface for the selectivity between the ClER and OER in 5 M NaCl. The OER versus ClER selectivity shifts from pure ClER at pH 0.9 toward OER and other parasitic reactions at pH 3.5.[103] For a ternary Ti–Ru–Ir oxide catalyst, the total Faradaic current responsible for the anodic reactions (OER and ClER) was found to increase with the increase in the Cl^- concentration (from 1 to 4 M), and 97% selectivity for ClER was achieved with the increased concentration of Cl^-. The local properties on the catalytic surface and the spatial distribution of catalytically active sites governed the selectivity, where increasing the RuO_2 amount increased the OER selectivity, and therefore, the ClER selectivity was decreased.[102] Although the majority of oxides (including IrO_2 and RuO_2) were more selective toward ClER than OER, especially in acidic electrolytes due to the favorable kinetics, thin MnO_x films on glassy-carbon-supported IrO_x exhibited high selectivity toward OER. Despite being electrocatalytically inactive, MnO_x selectively prevented the diffusion of Cl^- while accelerating the diffusion of water, protons, and O_2 between IrO_x and the electrolyte, facilitating the OER. The selectivity for ClER decreased from 86% to less than 7% in the presence of 30 mM Cl^-. While the real concentration of Cl^- ions (0.5 M) in seawater is several orders of magnitude higher than 30 mM, using such a high concentration would hinder fundamental studies of ClER due to interference from

https://doi.org/10.1021/acselectrochem.5c00381
ACS Electrochem. 2026, 2, 43–67

Scheme 3. Schematic Illustration Showing Impurity Effects during Seawater Electrolysis

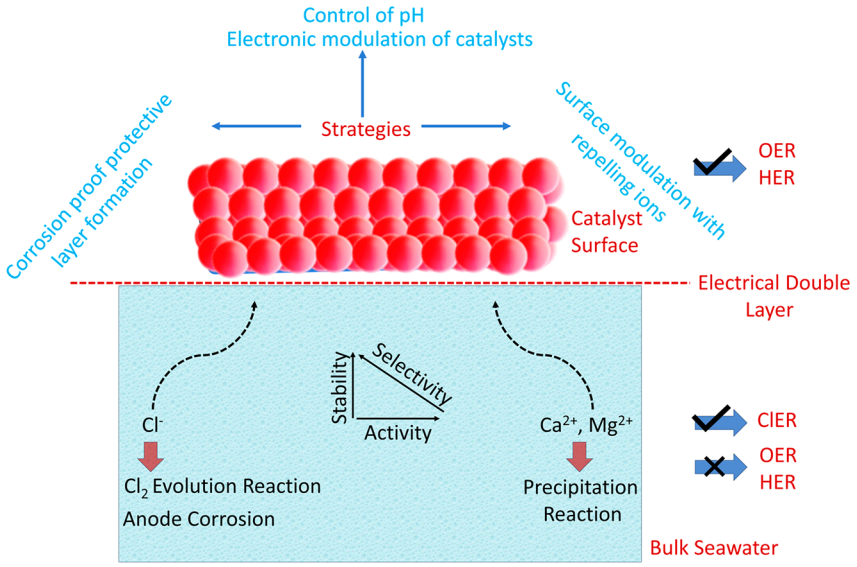

bubble formation and noise.[104] As mentioned earlier, the CrO_x layer increased the local pH at the electrode surface, which acted as an electrical barrier to repel Cl^- and thus favored OER over ClER.[99]

Li *et al.* mitigated Cl^--induced corrosion by designing a multilayered oxygen evolution electrode (MOEE) consisting of the NiFe-alloy substrate as the core layer, a corrosion-proof interlayer of $NiFeB_x$ to protect against ClER, and an OER-active surface layer of oxidized NiFeB. When the electrocatalytic OER activities of both MOEE and NiFe-alloy were tested in both 1 M KOH and 1 M KOH + 0.5 M NaCl, the electrocatalytic activity and stability of MOEE in 1 M KOH + 0.5 M NaCl surpassed those of NiFe-alloy. The OER activity of MOEE was sustained for 70 h, whereas that for NiFe-alloy decreased within 10 h due to the oxidative corrosion by Cl^- anions. The FE of the MOEE was maintained at 100% for OER, keeping the Cl^- ions in the electrolyte constant.[105]

Sulfate ions are repelled from Cl^- ions by electrostatic force, and thus, they decrease the ClER efficiency in seawater. Sulfate ions can be generated by their intentional addition in Cl^--containing electrolyte or by partial sulfurization of the catalyst surface. Hydrothermally fabricated NiFe-LDH on a Ni foam anode showed improved stability both in 1 M NaOH + 0.5 M NaCl and in 1 M NaOH + seawater in the presence of SO_4^{2-} at a current density of 400 mA cm^{-2} when coupled with a Pt cathode. The partially sulfurated Ni_2Fe-LDH/$FeNi_2S_4$/NF exhibited corrosion resistance toward Cl^- in 1 M KOH + 0.5 M NaCl due to the formation of a sulfate layer that caused electrostatic repulsion for the Cl^- ions, thereby improving the efficiency of the anode.[106]

2.3.3. Trends Observed in Seawater Splitting Due to the Contaminants. In seawater splitting, the performance of catalysts is significantly influenced by the presence of major ionic contaminants, such as Ca^{2+}, Mg^{2+}, and Cl^-, which impact both the cathodic and anodic processes (Scheme 3). Below is a brief elaboration of the impacts:

Impact of Ca^{2+} and Mg^{2+} on the Cathode. In natural seawater or simulated seawater (e.g., 0.5 M NaCl), Ca^{2+} and Mg^{2+} ions precipitate as $Ca(OH)_2$ and $Mg(OH)_2$, respectively, near the cathode surface due to the localized increase in the OH^- concentration during HER. These precipitates block the active catalytic sites, reducing the accessibility of reactants and thereby decreasing the overall efficiency of HER.[96] Furthermore, the accumulation of these hydroxides led to an increase in the local bulk pH, which can shift the reaction mechanisms and potentially destabilize the electrode material.

Impact of Cl^- at the Anode. At the anode, Cl^- ions compete with OH^- ions for adsorption on the catalyst surface. This competition hinders the OER, as the adsorption of Cl^- blocks sites that are essential for OH^- binding and subsequent oxidation. Cl^- adsorption not only reduces the activity and selectivity for the OER but also accelerates corrosion and degradation of the catalyst material, especially under high anodic potentials. In addition, Cl^- may favor the ClER, further reducing the efficiency and selectivity for OER.[100]

pH-Dependent Effects. Both the precipitation of $Ca(OH)_2$ and $Mg(OH)_2$ at the cathode and the adsorption of Cl^- at the anode are strongly influenced by pH.[96] An increase in local pH at the cathode regulates the hydroxide precipitation, whereas at the anode, pH affects the relative adsorption energies of Cl^- and OH^-. This interplay can dictate the balance between the ClER and the OER.

2.3.4. Strategic Interventions. EDL Modulation. The EDL is a structured region of charged species formed at the interface of a charged surface (here the electrode) and a liquid (here the electrolyte). The EDL governs the kinetics and mechanism of electrocatalytic reactions.[107] Optimizing the ionic distribution near the electrode surface can help to minimize the negative effects of contaminants. For example, applying suitable surface charges or using additives to modify the ionic environment can reduce the interactions of Ca^{2+}, Mg^{2+}, and Cl^- with the catalyst.[99]

Catalyst Surface Engineering. Designing catalyst surfaces with tailored hydrophilicity, specific adsorption sites, or antifouling properties can limit the blocking effects of $Ca(OH)_2$ and $Mg(OH)_2$ precipitates and reduce Cl^- adsorption. Protective coatings ($NiFeB_x$) or introduction with oversaturated nitrogen can also enhance stability and selectivity.[98,105]

By strategically addressing the parasitic chemical and electrochemical reactions associated with Ca^{2+}, Mg^{2+}, and Cl^-, it is possible to improve the overall efficiency and durability of seawater splitting systems. This approach is critical for

https://doi.org/10.1021/acselectrochem.5c00381
ACS Electrochem. 2026, 2, 43−67

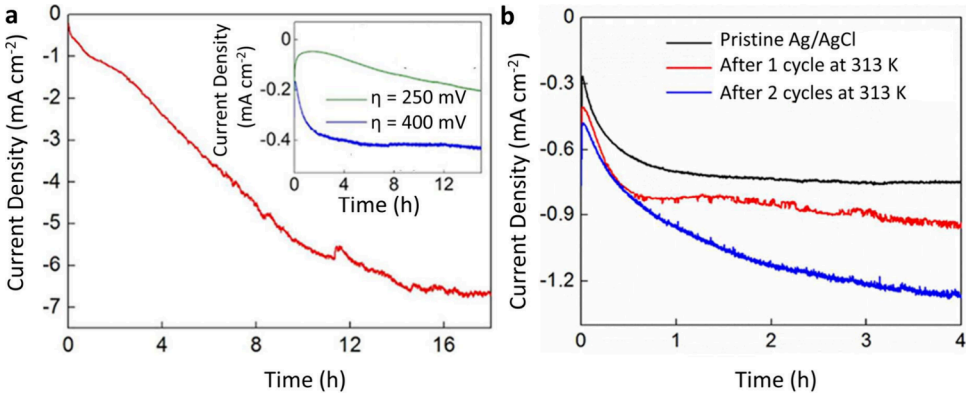

Figure 5. (a) Comparison of the current densities for the HER at a glassy carbon working electrode in 1 M H_2SO_4 obtained using a Ag/AgCl reference electrode at 540 mV overpotential for the HER (main panel, red line) and at 400 and 250 mV overpotential (inset, blue and green lines, respectively). (b) Comparison of the current densities for the HER at room temperature at a glassy carbon working electrode in 1 M H_2SO_4 obtained by using a Ag/AgCl reference electrode at 540 mV overpotential. Before each experiment, the Ag/AgCl reference electrode had been treated as follows: pristine (black line), used in single bulk electrolysis in 1 M H_2SO_4 at 313 K for 90 min (red line), and used in two bulk electrolyses in 1 M H_2SO_4 at 313 K, each for 90 min (blue line). The reference electrode was thoroughly rinsed and cooled to room temperature after each experiment at an elevated temperature. Adapted from ref 108. Copyright 2016 American Chemical Society.

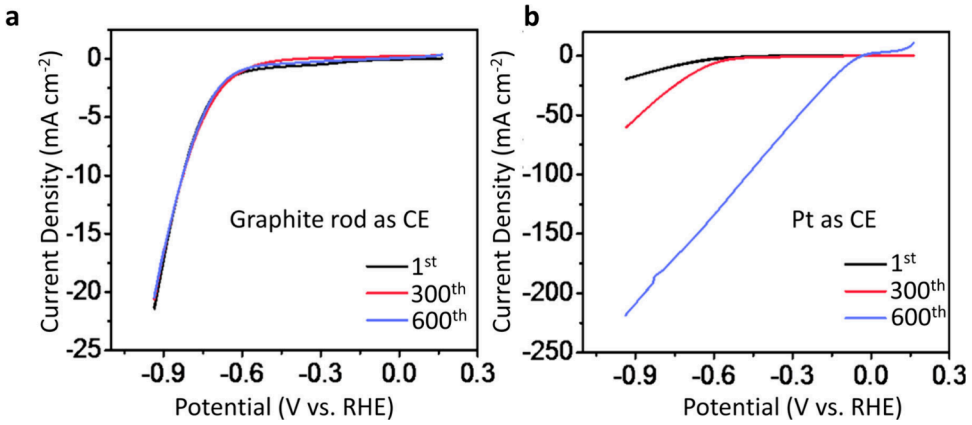

Figure 6. HER polarization curves of carbon cloth in 0.5 M H_2SO_4 with (a) a graphite rod and (b) a Pt plate as the counter electrode (CE). Adapted from ref 109. Copyright 2017 American Chemical Society.

advancing the scalability and sustainability of seawater electrolysis technologies.

3. CONTAMINANTS FROM REFERENCE ELECTRODES

Electrochemical measurements of water oxidation and reduction are typically conducted within a three-electrode configuration, employing a working electrode, a reference electrode, and a counter electrode. It is imperative that the potential of the reference electrode remain consistently stable and that the durability of this electrode be meticulously upheld to prevent any potential erroneous estimations of overpotential.

In this context, Roger and Symes had reported the impact of an $Ag/AgCl/Cl^-$ reference electrode on HER.[108] For this purpose, a three-electrode system was selected, comprising a glassy carbon electrode as the working electrode, a graphite rod as the counter electrode, and $Ag/AgCl/Cl^-$ as the reference electrode. These components were immersed in a 1 M H_2SO_4 solution. While the glassy carbon electrode was anticipated to maintain a current density of no more than 0.1 mA cm^{-2} at an overpotential of 540 mV, it exhibited a current density exceeding 5 mA cm^{-2} at the same overpotential following an extended period of electrolysis. This phenomenon was attributed to migration of Ag^+ ions from the reference electrode into the electrolyte and their subsequent *in situ* electrodeposition onto the working electrode (Figure 5a). The extent of this occurrence was largely dependent on the solubility of the ions within the electrolyte. Notably, the augmentation in the electrolysis temperature from 293 to 313 K notably accentuated this rise in current density due to the enhanced solubility of Ag^+ ions (Figure 5b). The contamination arising from the commercially available $Ag/AgCl/Cl^-$ reference electrode can contribute to a current density for HER on the order of 5 mA cm^{-2} at almost 500 mV overpotential due to the leakage of Ag^+ and redeposition on the working electrode. This current density becomes considerable and unavoidable for some cathode catalysts, which reach an approximately similar current density at this overpotential. To circumvent this issue, following steps can be considered: (i) the use of an alternative acidic electrolyte (e.g. phosphoric acid) in which the solubility product of the corresponding salt is much lower; (ii) the use of an appropriate reference electrode such as Hg/Hg_2SO_4 or the use of a "double junction" $Ag/AgCl/Cl^-$ reference electrode to prevent Ag^+ leakage and Ag contamination.[108]

https://doi.org/10.1021/acselectrochem.5c00381
ACS Electrochem. 2026, 2, 43−67

Table 4. Advantages and Limitations of Different Characterization Techniques

technique	advantages	limitations
ICP-MS[121]	1. Ability to identify types and composition of elements in complex samples such as crude oil, soil, etc.	1. Limited tolerance of total dissolved solids
	2. Highly sensitive technique	2. Destructive technique
ICP-OES[121]	1. Ability to identify types and composition of elements in complex samples such as crude oil, soil, etc.	1. Destructive technique
	2. Greater tolerance of total dissolved solids	2. Samples must be aerosolized
		3. Poor precision
XPS[122]	1. This technique can be used to identify surface composition and electronic states of the elements and is applicable in determining structure−property relationships in the field of electrocatalysis and photocatalysis	1. Due to the use of a high-energy X-ray probe, the cross section of the molecular orbital and valence band interaction is very weak
		2. Surface technique, limited to analyzing a few nanometers (5−10 nm) on the catalyst surface; requires sputtering by Ar^+ ions for depth analysis
		3. High vacuum is necessary
AFM[123]	1. High resolution and easy sample preparation	1. Expensive consumables
	2. Ability to identify magnetic domain structure	2. Unable to identify the chemical composition of a sample
STEM-EELS[124]	1. Provides chemical composition, oxidation states	1. Requires ultrathin samples
	2. Atomic-scale resolution	2. High-cost equipment is needed, and it is difficult to handle
		3. Mostly probes local or surface regions due to short inelastic mean free path of electrons causing energy loss phenomenon near the surface of the materials rather than in the bulk
In situ Raman spectroscopy[125,126]	1. Nondestructive technique	1. Interference of fluorescence signals
	2. Can probe liquids, solids, and gases	2. Limitation of surface materials: strong signals for *in situ* Raman can only be achieved in Au, Ag, and Cu substrates
	3. Identification of surface-bound molecules and intermediates to decipher the reaction mechanism	3. Primarily surface-sensitive, with the penetration depth limited to a few hundred nanometers depending on the material

4. CONTAMINANTS FROM COUNTER ELECTRODES

For any electrochemical reaction, the counter electrode should possess the traits of chemical inertness, mechanical stability, and high electrical conductivity to facilitate the efficient flow of electrons. While Pt is renowned for being a prominent choice due to its chemical resistance to oxidation, it still exhibits limitations.[109] Under specific chemical and electrochemical circumstances, Pt can display reactivity. The dissolution of Pt hinges on factors such as the electrocatalyst's characteristics/type, the relative catalytic area between the working and counter electrodes, the potential window, and the scan rate on the working electrode. Notably, this dissolution was more pronounced in acidic electrolytes compared with alkaline ones. This phenomenon was initially observed by Ota *et al.* in 1988, who noted systematic weight loss of the Pt counter electrode in acidic electrolytes due to dissolution followed by redeposition on the working electrode.[110] Chen *et al.* conducted two separate experiments employing bare carbon cloth as the working electrode and a Pt or graphite rod as the anode in 0.5 M H_2SO_4.[109] Following 600 CV cycles, the HER activity of the carbon cloth approached that of Pt. This was attributed to the formation of Pt nanodots on the carbon cloth. Notably, the HER activity of carbon cloth remained unchanged when a graphite rod was utilized as the counter electrode (Figure 6).[109]

Wei *et al.* also suggested that the electrocatalytic activity of a graphite rod became comparable to that of commercial Pt/C following 13,000 CV cycles when Pt wire was employed as a counter electrode. The plausible mechanism of Pt dissolution involves several steps: (1) adsorption of water or OH^- during HER on the counter electrode; (2) displacement between O and Pt atoms; (3) weakening the interaction between Pt atoms and surface counterparts; and (4) Pt atom dissolution. The transfer of Pt from the counter electrode to the working electrode is heavily reliant on the relative area of the counter electrode to the working electrode. Precisely, the electrochemically active surface area of the counter electrode should be 10 times larger than that of the working electrode.[111] Hasan and Allam clarified that if the area of the Pt counter electrode remained constant and the area of the working electrode increased from 0.25 cm^2 to 1 cm^2, there was a significant drop in overpotential for HER. This stems from the escalation of Pt dissolution and deposition on the working electrode.[112] Therefore, to mitigate the unavoidable effects of Pt dissolution (both chemical and electrochemical) and redeposition on the working electrode, the use of Pt as a counter electrode must be avoided. In this context, a substitute counter electrode should meet the following criteria: (i) the counter electrode should be stable, e.g., graphite rod; (ii) the counter electrode should have a high surface area to conduct the sluggish four-electron OER during HER at the cathode.[109] If Pt is used as a counter electrode, then an ion exchange membrane or glass frit should be used during the HER.

5. CONTAMINANTS FROM DISSOLUTION OF WORKING ELECTRODES (SUBSTRATES) AND CATALYSTS

Electrocatalytic water splitting in freshwater systems under industrial conditions (high electrochemical potentials, elevated temperatures, and overextended durations) could lead to the dissolution, leaching, and corrosion of electrocatalyst materials and their supporting substrates. For example, work on NiFe-LDH OER catalysts in alkaline freshwater (1 M KOH) demonstrated noticeable metal leaching. As reported by Li *et al.*, post-operation FESEM analysis showed decrease of nanosheets due to catalyst leaching after 12 h continuous OER.[113] Among Ni-based alloys, NiMo alloy is a promising candidate for HER.[15] The leaching of Mo causes surface roughening of the electrode with the formation of molybdate species, resulting the improvement in HER activity.[114] Substrate materials such as nickel foam, stainless steel mesh, and titanium are universally susceptible to corrosion and leaching under rigorous freshwater splitting. Colli *et al.* documented that when SS316L stainless steel was used as an anode and OER was

https://doi.org/10.1021/acselectrochem.5c00381
ACS Electrochem. 2026, 2, 43−67

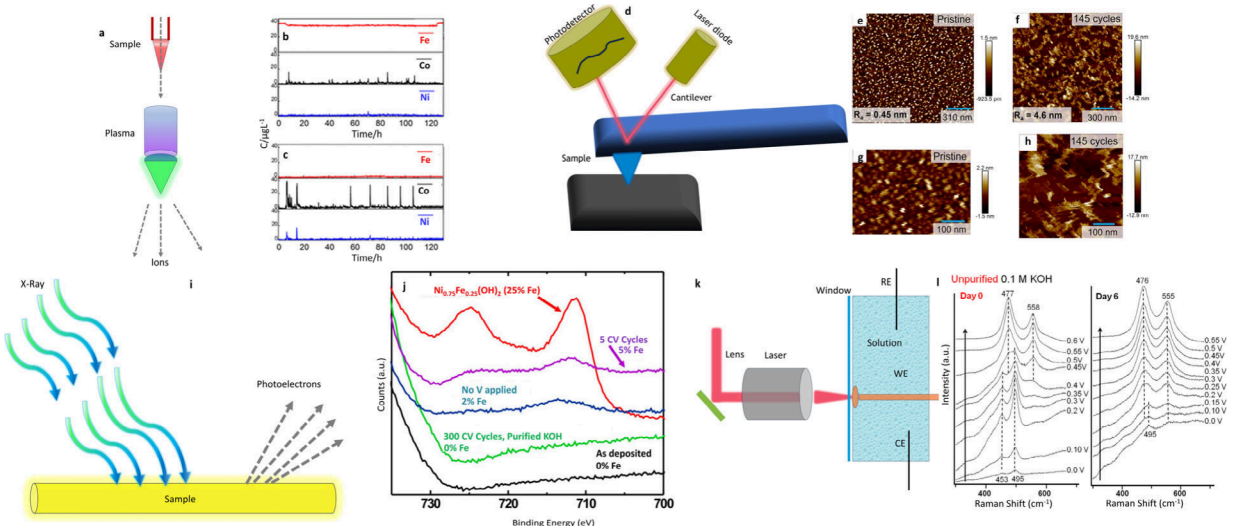

Figure 7. (a) Schematic of major components of the ICP-MS and ICP-OES instrument. (b, c) ICP-OES transient analysis of the corrosion products of the Ni−Co_3O_4 catalyst in (b) a 1 M KOH Fe-contaminated and (c) Fe-free KOH solution. The Fe content of the KOH solution was monitored. Adapted from ref 61. Copyright 2019 American Chemical Society. (d) Schematic of an AFM instrument. (e−h) Atomic force microscopy images of (e, g) pristine epitaxial LNO film (note different scales) and (f, h) the same film after cycling 120 times in Fe-free 1 M KOH followed by 25 times in 100 ppb Fe-spiked 1 M KOH. The arithmetic average roughness is given by R_a and indicates that cycling causes topological restructuring. Adapted with permission from ref 24. Copyright 2024 Elsevier. (i) Schematic of XPS analysis. (j) XPS Fe 2p spectra for $Ni(OH)_2$/NiOOH thin films after five CV cycles in Trace Select KOH (purple), 12 min in TraceSelect KOH electrolyte with no applied potential (blue), and 300 CV cycles in purified KOH (green). Spectra for an as-deposited film containing no Fe (black) and a film with 25% co-deposited Fe (red) are shown for reference. The increase in the intensity for binding energies above ∼730 eV is due to the onset of a KLL Auger peak. Spectra are offset on the *y* axis for clarity. Adapted from ref 62. Copyright 2014 American Chemical Society. (k) Schematic of *in situ* Raman cell. (l) *In situ* Raman spectra collected over $Ni(OH)_2$/NiOOH films deposited on roughened Au in unpurified 0.1 M KOH on Day 0 and Day 6. Potentials are reported vs Hg/HgO. The oxygen evolution equilibrium potential is 0.365 V vs Hg/HgO in 0.1 M KOH. Adapted from ref 58. Copyright 2015 American Chemical Society.

carried out at a current density of 300 mA cm^{-2} in 6 M KOH at 75 °C, there was slight release of Fe, and Cr. However, for shorter time of experiments, a slight coloration of the clear electrolyte and simultaneous accumulation of black powder at the cathode were observed, might be attributed to the corrosion of the pristine electrode.[115] In highly concentrated chloride environments like in seawater, Cl^- ions disrupt the protective TiO_2 layer on Ti substrates by penetrating and adsorbing into oxygen vacancies, making the film porous and less protective, which facilitates pitting corrosion and compromises the integrity of the Ti surface.[116] These challenges of dissolution and leaching in freshwater electrolytes are further increased by the presence of seawater. The natural abundance of chloride and other halide ions in seawater profoundly accelerates the corrosion and leaching mechanisms identified above, as demonstrated by Yang *et al.*[117] and Li *et al.*[113] In alkaline seawater electrolytes, electrode corrosion rate can increase due to accelerated breakdown of passive surface oxides, and halide-induced attack, resulting in even more rapid catalyst and substrate degradation.[113,117,118] Br^- ions further lower the energy barrier for metal dissolution and inflict distinct morphological and compositional changes compared to freshwater operation.[119,120]

6. CHARACTERIZATION METHODS

The influence of contaminants and impurities on electrocatalytic water splitting reactions, particularly the OER and HER, is assessed through various electrochemical parameters such as the overpotential, Tafel slope, electrochemically active surface area, TOF, mass activity, etc. To thoroughly investigate the structural and electronic changes that occur at the electrodes due to the presence of contaminants, both *in situ* and *ex situ* characterization methods beyond electrochemical techniques are essential. Recent advancements have shed light on the structural evolution, degradation processes, and reaction mechanisms of electrocatalysts in water splitting under the influence of contaminants using these characterization techniques. This section highlights the functional applications of some common characterization techniques used to monitor the structural evolution and catalytic pathways in the presence of contaminants. These include microimaging, X-ray-based techniques, and optical spectroscopies. These techniques have some advantages and limitations, which are summarized in Table 4.

6.1. ICP-OES. ICP-OES can investigate the corrosion resistance of a catalyst by detecting the ion concentration of active metals in the electrolyte. The basic instrumentation of the ICP-OES is described in Figure 7a. Moreover, in the case of electrolytes containing contaminants, ICP-OES can determine the variation in the concentration of the contaminants. For instance, the composition of $Ni(OH)_2$ after electrolysis in an unpurified KOH electrolyte was determined by the ICP-OES technique. In this unpurified electrolyte, the Ni-containing film (∼30 nm thick) consisted of ∼5% Fe after just 12 CV cycles. The Fe content increased to 23−26% of the total metal in the film after extended aging (38 days). The Fe content of the film appears to increase logarithmically with aging time, and the Fe contents determined from XPS and ICP-OES were similar.[58] For the $LaNiO_3$ perovskite structures, the amount of Fe was determined by analyzing ICP-MS after spiking Fe at a particular time interval in purified KOH. During chronoamperometry at 1.7 V vs RHE, a similar amount of Fe was spiked in purified 1 M KOH electrolyte in a specific time interval, and an aliquot of the electrolyte was taken for ICP-MS analysis to determine the adsorbed Fe on the perovskite surface and correlate it with the increase in the OER activity. The decreasing concentration of Fe

https://doi.org/10.1021/acselectrochem.5c00381
ACS Electrochem. 2026, 2, 43−67

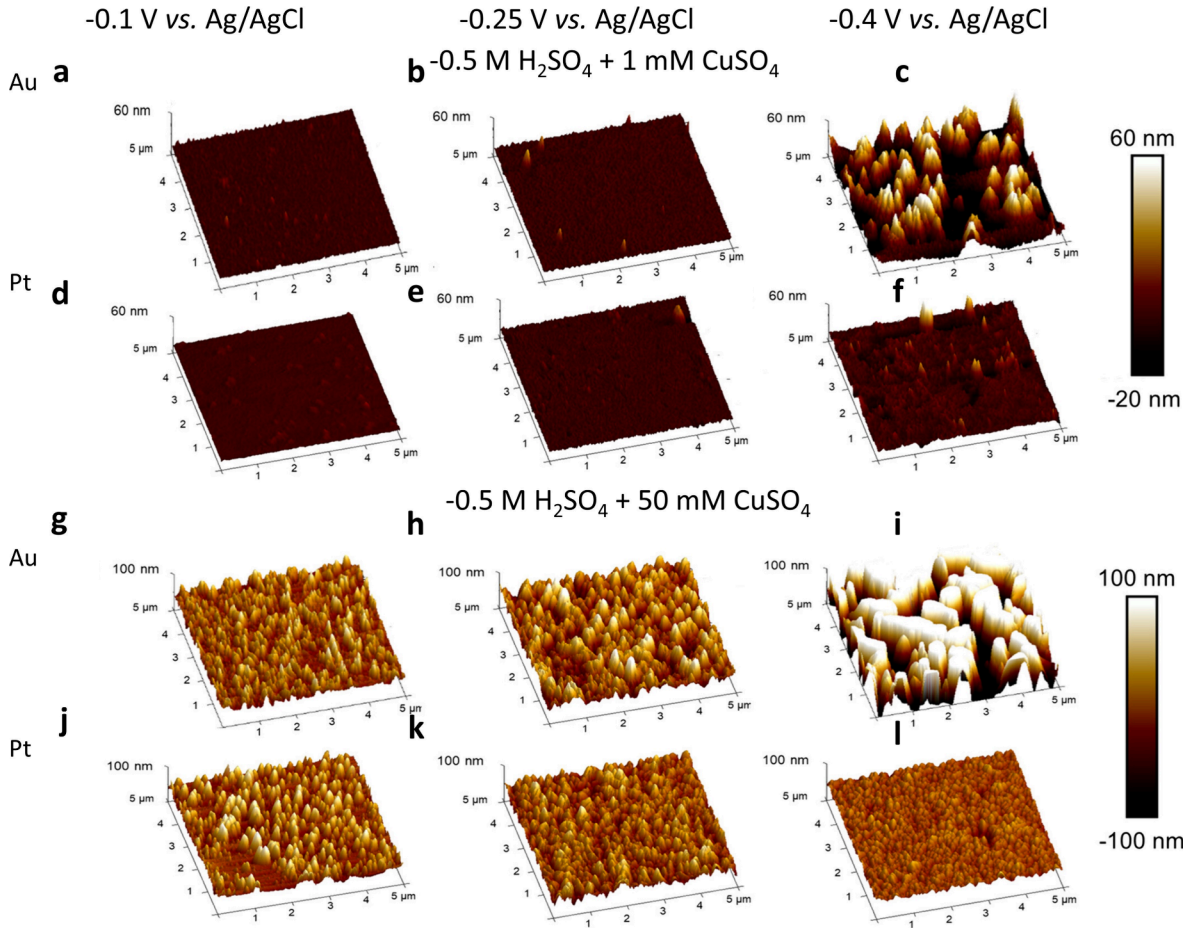

Figure 8. (a–f) AFM 3D height scans of Au electrodes in 0.5 M H_2SO_4 with 1 mM $CuSO_4$ electrolyte swept to and held for 5 min at (a) −0.1 V vs Ag/AgCl, (b) −0.25 V vs Ag/AgCl, and (c) −0.4 V vs Ag/AgCl and of Pt electrodes in the same electrolyte swept to and held for 5 min at (d) −0.1 V vs Ag/AgCl, (e) −0.25 V vs Ag/AgCl, and (f) −0.4 V vs Ag/AgCl. (g–l) AFM 3D height scans of Au electrodes in 0.5 M H_2SO_4 with 50 mM $CuSO_4$ electrolyte swept to and held for 5 min at (g) −0.1 V vs Ag/AgCl, (h) −0.25 V vs Ag/AgCl, and (i) −0.4 V vs Ag/AgCl and of Pt electrodes in the same electrolyte swept to and held for 5 min at (j) −0.1 V vs Ag/AgCl, (k) −0.25 V vs Ag/AgCl, and (l) −0.4 V vs Ag/AgCl. Adapted from ref81.

in the electrolyte indicated the adsorption of Fe on the $LaNiO_3$ surface, which increased the OER activity.[24] Shi *et al.* investigated the amount of adsorbed anion (SeO_3^{2-}) on the surface of the $Ni(OH)_2$ electrode by ICP-MS, which in turn enhanced the OER activity in an electrolyte of 1 M KOH + SeO_3^{2-}.[39]

6.2. *In Situ* ICP-OES. The *in situ* combination of ICP-OES with an electrochemical cell was investigated to analyze the concentration of leached cations as well as the contaminant ions during a constant electrochemical experiment.[61] Spanos *et al.* investigated the concentration of dissolved metal species of Co and Ni and the Fe in the KOH electrolyte during a constant chronopotentiometry stress test at 10 mA cm^{-2} for 2 h by combining electrochemical flow cell (EFC) measurements with online ICP-OES corrosion investigations.[61] The Fe concentration, which was 40 $\mu g\ L^{-1}$ before applying the chronopotentiometry stress, was observed to decrease in 2 h. Moreover, in the presence of Fe in the KOH electrolyte, there was a minimal signal for Ni and Co in the electrolyte, whereas it was significantly increased in purified KOH, implying the corrosion of the electrode. This was directly correlated to the OER activity of Ni–Co_3O_4 catalysts, where the adsorbed Fe not only enhanced the electrocatalytic OER activity but also restricted the leaching of Ni and Co from the catalyst under the current stress (Figure 7b,c).[61]

6.3. STEM-EELS. High-angule annular dark-field (HAADF)-STEM is widely used for understanding the location of different atoms in materials due to the atomic-level resolution and atomic-number contrast.[127] In addition, EELS in STEM has become a powerful method for atomic-scale chemical identification and measurement of bonding information, although EELS provides only localized information that may not fully represent bulk information.[128] For LSCO-30 ($La_{0.7}Sr_{0.3}CoO_3$) and LCO ($LaCoO_3$) catalysts, STEM and EELS were employed to investigate surface and electronic structural changes after cycling in purified 0.1 M KOH with and without 0.1 ppm Fe contaminants. STEM imaging revealed progressive surface amorphization and oxygen vacancy formation both in LCO and LSCO-30, where contrast variations in Co–O layers became more pronounced after cycling in Fe-containing KOH. EELS analysis revealed reduction in the Co valence state and a decrease in O K-edge prepeak intensity at 530 eV, which is consistent with the increased oxygen vacancy formation. The effect of surface amorphization and surface reconstruction was more noticeable for LSCO-30 catalysts.

For LSCO-30, Fe accumulation was detected near Co-rich regions, as Fe L-edge EELS suggested a higher surface Fe

https://doi.org/10.1021/acselectrochem.5c00381
ACS Electrochem. 2026, 2, 43–67

concentration without significant chemical state changes.[64] Additionally, EELS characterization of *in situ*-generated Co-KOH and CoFe-KOH catalysts indicated that both catalysts exhibited a Co^{2+} oxidation state, and the Co $L_{3,2}$ fine structure was consistent with the electronic modulation upon Fe incorporation into the Co host lattice.[70]

6.4. AFM. Scanning probe microscopy (SPM) employs a physical probe to meticulously scan the surface of a material, producing high-resolution imagery and in-depth data concerning its topography, chemical composition, surface roughness, and various physical properties. Among the SPM techniques, AFM stands out by utilizing mechanical interactions between the probe and the sample surface, enabling exceptionally precise surface characterization and analysis.[129] The basic instrumentation of the AFM is shown in Figure 7d.

AFM is an important tool for examining the surface topology of an electrode with extremely high spatial resolution up to the atomic level. The surface topology of the electrochemically cycled epitaxial LNO film after spiking an external Fe contaminant was observed by comparison with the AFM of the pristine epitaxial LNO. The cycled epitaxial LNO film was prepared after cycling 120 times in Fe-free 1 M KOH followed by 25 times in 100 ppb Fe-spiked 1 M KOH. The AFM scans showed almost a 10-fold increment of the roughness of the Fe-spiked LNO film compared with the pristine one due to the formation of $Ni_zFe_{1-z}O_xH_y$ or FeO_xH_y (Figure 7e–h).[24] The effect of Cu^{2+} impurities during HER in acidic electrolyte was systematically investigated by Saini *et al.* across different applied voltages, Cu^{2+} concentrations, and working electrodes (Au and Pt).[81] AFM was employed to observe the changes in the surface topology under these different conditions. For both Pt and Au working electrodes, when 1 mM Cu^{2+} was present in the electrolyte, very little copper deposition was observed on the electrode surface at −0.1 V vs Ag/AgCl, whereas with increasing the cathodic voltage to −0.25 and −0.4 V vs Ag/AgCl, the deposits became taller. However, the deposition was more fine-grained for Pt than for Au. When the impurity concentration was increased to 50 mM, the deposition intensified for Au and followed a similar increasing trend with increasing cathodic voltage, with the grain size reaching 1 μm at the potential of −0.4 V vs Ag/AgCl. In contrast, although Pt showed enhanced deposition with increasing concentration at −0.1 and −0.25 V vs Ag/AgCl, at −0.4 V vs Ag/AgCl it exhibited decreased deposit height. This phenomenon is attributed to the strong competition between Cu deposition and HER on electrocatalytically active Pt (Figure 8).[81]

6.5. XPS. XPS is a critical characterization technique for analyzing the electronic state of the elements, chemical shifts in a composite or heterostructure, and the surface composition of the catalysts. XPS is particularly effective within a depth of less than 10 nm. However, by employing Ar^+ ion sputtering, the surface properties beyond 10 nm can be evaluated.[130] Moreover, XPS is crucial in identifying the cationic and anionic vacancies on the surface, which may result from doping with secondary elements, the incorporation of foreign elements appearing from electrolytes, or the presence of extrinsic contaminants. The basic technique of XPS is described in Figure 7i.

As already discussed in the previous OER section, Fe is the most common impurity present in KOH, and it is responsible for enhancing the OER activity. Even after using the highest-purity KOH electrolyte and high-purity $Ni(NO_3)_2$ (99.999%), Fe was deposited on the $Ni(OH)_2$ catalysts. After five CV cycles at a rotation rate of 1500 rpm, Fe appeared to be incorporated in the $Ni(OH)_2$ film/GC-RDE, which could be correlated by XPS. The atomic ratio of Ni and Fe was observed to be 95:5 at the surface, although XPS depth profiling suggested that Fe was incorporated not only at the surface but also throughout the catalyst film due to the electrolyte-permeable structure. However, there was no signal of Fe after 300 CV cycles in purified KOH (Figure 7j).[62] Besides, cations and anionic contaminants could also improve the OER activities of transition metal hydroxide catalysts. For instance, the presence of SeO_3^{2-} in the KOH electrolyte improved the OER activity of the $Ni(OH)_2$ catalyst. The valence state of adsorbed Se on the surface of the catalyst after OER was observed to increase, as shown by XPS.[39] The trace amounts of Fe and Ni in the electrolyte exhibited a noticeable impact on the HER activity of the catalysts, especially on the Cu catalyst, which used to have an inferior HER activity compared with Ni and Fe. Li *et al.* tested the HER activity on a Cu RDE in 99.99% 0.1 M NaOH (containing 40 nM Fe and 160 nM Ni) and 99.99% 0.1 M CsOH (containing 240 nM Fe). After 1.9 h of electrolysis of the Cu RDE in 0.1 M CsOH and 0.1 M NaOH at −0.6 and −0.68 V vs RHE, the Fe signal was observed in XPS only in the case of 0.1 M CsOH, while in 0.1 M NaOH the Ni and Fe counts were below the detection limit of XPS.[85]

6.6. *In Situ* Raman Spectroscopy. Raman spectroscopy is a powerful analytical tool to provide detailed molecular fingerprinting and insight into the reaction mechanism. Raman spectroscopy is a scattering technique based on the Raman effect, where the frequency of a small fraction of scattered radiation differs from that of the monochromatic incident photons due to inelastic scattering by molecular vibrations. A monochromatic laser beam interacts with a sample, and the inelastically scattered light generates a Raman spectrum.[131]

The scattered light primarily consists of Rayleigh scattering (same frequency as incident radiation) and a smaller fraction of Raman scattering (different frequency). Stokes lines appear when the scattered frequency is lower, while anti-Stokes lines occur when it is higher. Stokes bands, being more intense, are commonly measured, while anti-Stokes bands are preferred for fluorescing samples. The Raman shift is independent of the incident radiation's wavelength but requires a change in molecular polarizability during vibration.[132]

Electrochemical *in situ* Raman measurements are particularly valuable for elucidating the structural reconstruction of the catalysts and evolution of reaction intermediates during electrochemical processes.[133] The basic instrumentation of the *in situ* Raman cell is described in Figure 7k. The effect of the Cu^{2+} impurity in 1 M KOH during the OER was examined on the Ti plate by increasing the number of CV cycles. A peak corresponding to $Cu(OH)_2$ emerged during the OER cycling, with the intensity increasing as the number of cycles increased. The increase in current density was related to this fact. A similar experiment was conducted by varying the applied anodic potential. At a potential of 0.77 V vs RHE, there was no characteristic Raman peak of $Cu(OH)_2$, which appeared at a potential of 0.82 V vs RHE, and the intensity continued to increase up to a potential of 1.07 V vs RHE.[23]

The phase transformation of the $Ni(OH)_2$/NiOOH structure with and without Fe contaminants in 0.1 M KOH was investigated using *in situ* Raman by Klaus *et al.* The *in situ* Raman spectra were investigated for multiple sequential days.[58] The characteristic Raman vibrations of β-$Ni(OH)_2$, α-$Ni(OH)_2$, and γ-NiOOH were observed at wavenumbers of 445–449, 460–465, and 555–560 cm^{-1}, respectively. The 480 cm^{-1}/560

https://doi.org/10.1021/acselectrochem.5c00381
ACS Electrochem. 2026, 2, 43–67

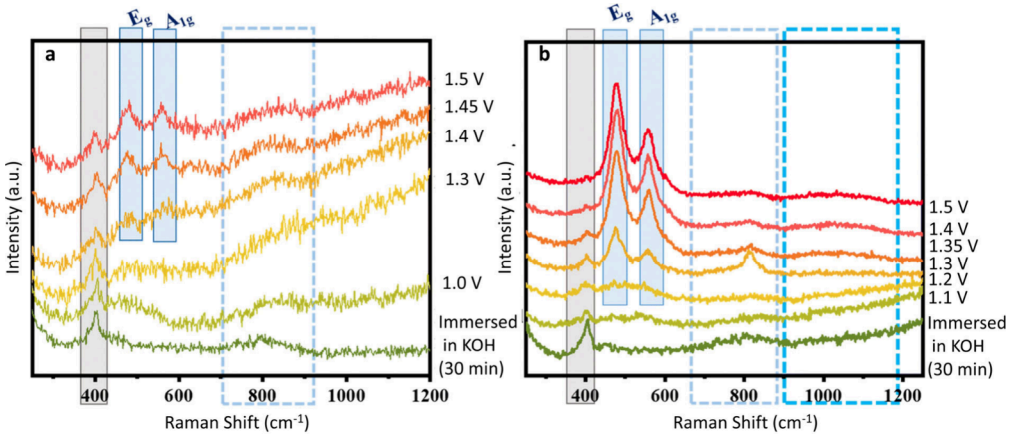

Figure 9. (a) In situ Raman spectra of $LaNiO_3$ collected during the OER process (1.0−1.7 V vs RHE) in 1 M purified KOH and (b) with the addition of Fe impurities. Adapted from ref 134. CC BY 3.0.

cm^{-1} peak height ratio was observed in the initial samples and after 6 days of aging in both purified and Fe-containing electrolytes. Initially, the peak height ratio was 1.55 in both electrolytes. However, after aging for 6 days at a potential of 0.6 V vs Hg/HgO, the peak height ratio was pronouncedly decreased in the case of unpurified electrolyte, which was not only attributed to the formation of NiOOH but also due to the construction of an oxidized form of NiFe-LDH (Figure 7l).[58]

$Ni(OH)_2$ also exhibited a striking improvement in the OER activity in the presence of an anionic contaminant like 0.1 M SeO_3^{2-}. The potential-dependent structural evolution of $Ni(OH)_2$ in 1 M KOH + 0.1 M SeO_3^{2-} was investigated by *in situ* Raman analysis, which could also be corroborated with the XPS analysis discussed earlier. With the gradual increase in the potential, the peak at 452 cm^{-1} diminished, with the appearance and the gradual increase of new peaks at 475 and 555 cm^{-1}, implying the oxidation of $Ni(OH)_2$ to NiOOH. Due to the adsorption of SeO_3^{2-}, a characteristic peak corresponding to SeO_3^{2-} appeared at a wavenumber of 807 cm^{-1}, which was substituted with a new peak at a potential of 1.58 V vs RHE due to the oxidation of selenites to selenates, promoting the OER activity.[39] Similarly, the vibration modes of $LaNiO_3$ perovskite oxide were also found to be changed during the OER in the presence of Fe impurities in the electrolyte due to surface reconstruction and evolution. The characteristic band of $LaNiO_3$ appeared at 400 cm^{-1}, which corresponds to the presence of a NiO_6 octahedron. In purified KOH, the peak position remained unaltered, although its intensity decreased with an increase in the applied potential. Moreover, at 1.3 V vs RHE, two separate bands appeared at 474 and 555 cm^{-1}, which correspond to the bending and stretching vibration modes of Ni−O in Ni oxyhydroxide species, and the relative intensity ratio of 1.15 indicated the presence of γ-NiOOH species. In contrast, in the presence of Fe-contaminated KOH, the vibrational band at 400 cm^{-1} disappeared with increasing applied potential, signifying lattice distortion and surface amorphization. In the presence of Fe impurities, the relative and absolute intensities of these bands at 474 and 555 cm^{-1} changed dramatically, along with an increase in the relative intensity ratio to 1.41, with increased Fe incorporation (Figure 9).[134]

Thus, *in situ* Raman spectroscopy provides insight into the potential and time-dependent structural evolution of the catalysts in the presence of impurities in the electrolyte.

CONCLUSIONS

Extensive efforts have been devoted to designing and engineering catalysts with tailored physical and electronic properties through strategies such as doping, strain engineering, charge transfer modulation, and creation of heterogeneous interfaces. Beyond these intentional modifications, the presence of contaminants, whether deliberately introduced or inadvertently present, can significantly influence the OER and HER half-reactions and thus the overall water splitting process. These effects are especially important in the context of the desire to obtain H_2 from less-pure water sources, such as seawater.

In this review, we have comprehensively discussed the influence of contaminants and inherent ionic constituents on electrocatalytic water splitting and seawater splitting reactions. We summarized that the presence of trace metal cations and anions in the electrolytes can significantly influence the activity, selectivity, and stability of catalysts by altering the surface composition, interfacial charge dynamics, and electronic structure. The naturally present ionic species in seawater can critically impact both the cathodic and anodic parts of seawater splitting, giving rise to challenges like cathode fouling and the Cl_2 evolution reaction. The review has also highlighted that impurities originating from reference and counter electrodes can lead to unintended metal redeposition, surface reconstruction, and structural degradation, thereby either enhancing or deteriorating catalyst performance. Advanced characterization techniques such as ICP-OES, STEM-EELS, XPS, *in situ* Raman, and AFM have proven invaluable for identifying and elucidating these contaminant-induced structural and electronic modifications primarily occurring at or near the catalyst surface.

Key findings from our review are summarized below:

(1) For diverse catalysts, including transition metal oxides, hydroxides, and perovskite oxides, trace iron species often have a beneficial impact by the formation of iron-based mixed metal hydroxides or LDHs, thereby enhancing the OER performance.[24]

(2) The incorporation of cations that form insoluble hydroxide precipitates increases the overpotential for OER by inhibiting reaction kinetics.[57]

(3) Surface-adsorbed anions such as selenates and sulfates can reduce the OER overpotential by lowering the free energy of adsorption for reaction intermediates.[39]

https://doi.org/10.1021/acselectrochem.5c00381
ACS Electrochem. 2026, 2, 43−67

(4) The electrocatalytic HER activity is strongly sensitive toward the reduction potential and UPD potential of cations present in the electrolyte.[80]
(5) In seawater splitting, insoluble calcium and magnesium hydroxides precipitate on the cathode surface, causing cathode fouling and increased HER overpotential by blocking active sites.[96]
(6) Chlorine evolution during seawater splitting reduces the FE of OER, which can be mitigated by introducing chloride-repelling anions or protective surface layers.[100,105]
(7) Reference electrodes and counter electrodes can introduce contaminant ions (Ag^+, Pt^{2+}) that lead to inaccurate measurements of overpotential, affecting the reliability of electrocatalytic water-splitting studies.[108,109]
(8) Dissolution from the catalysts on the working electrode and from the substrate itself can cause degradation or improvement of the OER and HER activity in freshwater.[113,114] The leaching of metal ions was found to be accelerated in seawater electrolyte.[113,115,117]

This review underscores this critical but underexplored research area in electrocatalysis, summarizing the sources, mechanisms, and influences of contaminants in both seawater and pure water electrolysis. By providing an insightful understanding of contamination mechanisms and their impact on electrocatalytic activity, we aim to inspire innovative approaches for rational design of advanced materials for electrocatalysis with improved activity, stability, and selectivity for sustainable fuel production.

FUTURE PROSPECTS

Understanding contamination mechanisms and their mitigation is crucial for enhancing the stability and efficiency of electrocatalysts. Comprehensive studies on degradation pathways help uncover how contaminants such as metal ions, organic impurities, or byproducts influence the structure, surface chemistry, and performance of catalysts. By identification of these detrimental interactions, researchers can develop strategies to minimize contamination effects. Approaches such as advanced electrolyte pretreatment, protective catalyst coatings, and self-healing electrode designs offer promising solutions to extend catalyst longevity and maintain the efficiency.

Contamination also plays a significant role in the catalyst design. Insights gained from understanding poisoning and fouling mechanisms can guide the synthesis of more robust, contamination-resistant materials. Catalysts engineered to withstand impurity-induced degradation can improve performance in practical applications, ensuring reliability in real-world environments.

The development of advanced electrolytes is another crucial aspect of contamination mitigation. Research efforts are focused on preparing high-purity electrolytes that are either free from impurities or tolerant of specific contaminants. This is particularly relevant for large-scale water splitting, where seawater or wastewater often introduces unwanted elements. Addressing these challenges ensures compatibility with real-world water sources and enhances process efficiency in industrial applications.[135]

Scaling up electrochemical systems requires a deep understanding of contamination effects on long-term durability.[136] In commercial electrolyzers, impurity accumulation can lead to electrode degradation, reducing the operational lifespan. Exploring cost-effective solutions to mitigate contamination, such as improved electrolyte management or periodic regeneration techniques, can significantly lower operational costs and enhance the system viability for industrial-scale hydrogen production.

Future research directions may involve integrating AI and machine learning to predict contamination effects and optimizing adaptive control systems. These computational approaches can accelerate the identification of contamination sources and aid in the design of self-regulating catalytic systems. Additionally, emerging catalysts may be intentionally doped with controlled impurities to explore potential performance enhancements, offering new avenues for catalyst engineering.[137]

Beyond water splitting, contamination studies have broader implications for related electrochemical processes. Insights from contamination mechanisms in electrocatalysis can inform research on urea oxidation,[133] CO_2 reduction,[138] and nitrogen reduction reactions,[139] where similar fouling and poisoning effects may hinder catalyst performance. Addressing contamination challenges across these fields can contribute to the advancement of sustainable energy and chemical conversion technologies. The four major directions can be summarized as follows:

A. Rational Design of Impurity-Resistant Electrocatalysts. The development of electrocatalysts with improved resistance to contaminant-induced degradation is of great importance in robust catalyst engineering. Current approaches majorly focus on postsynthesis surface modifications or protective coatings, which often compromise catalytic activity or add processing complexity.[140] Research should prioritize possible *ab initio* design of electrocatalysts that integrate impurity resistance into fundamental electrocatalyst electronic and structural properties. This computational high-throughput screening combined with machine learning algorithms can accelerate the identification of catalyst compositions and crystal facets that exhibit minimal binding affinity for specific seawater contaminants (Ca^{2+}, Mg^{2+}, Cl^-) while maintaining optimal binding energies for OER and HER intermediates.[93,141] Also, by leveraging descriptor-based approaches that correlate electronic structure parameters (d-band center) with both catalytic activity and contaminant tolerance, it becomes easy to navigate the traditionally competing demands of performance and stability.[141]

B. Operando Characterization for Tracing Contaminants Interactions. A handful of published works generally rely on *ex situ* or *post-mortem* analysis, which fails to capture the dynamic, potential-dependent nature of contaminant interactions under catalytically active conditions. However, a mechanistic understanding of how contaminants modify reaction pathways, intermediate species, and electrode−electrolyte interfaces in real time is important for the development of targeted mitigation strategies. The implementation of multimodal *operando* characterization platforms combining spectroscopic (Raman spectroscopy, X-ray absorption spectroscopy (XAS)), microscopic (electrochemical scanning tunneling microscopy), and mass spectrometric techniques can be used to monitor the adsorption, incorporation, and desorption of contaminants during electrochemical reactions.[142,143] Capabilities like this make it possible to measure potentials of specific contaminants beginning to poison active sites, the mechanism of contaminant interactions that can alter the nature of rate-determining steps, and contaminants' preferential accumulation sites whether at grain boundaries or edges.

https://doi.org/10.1021/acselectrochem.5c00381
ACS Electrochem. 2026, 2, 43−67

Possible research should be focused on the following areas:

(1) development of specialized electrochemical cells compatible with synchrotron-based X-ray techniques for simultaneous measurement of oxidation state changes and contaminant distribution during freshwater and seawater electrolysis;

(2) implementation of *operando* differential electrochemical mass spectrometry (DEMS) with isotopic labeling to distinguish between HER/OER products and side reactions involving contaminants (e.g., chlorine evolution);

(3) establishment of *operando* atomic force microscopy protocols to track surface morphology evolution and deposit formation;

(4) creation of open-access databases cataloging *operando* spectroscopic signatures of common contaminant−catalyst interactions to facilitate rapid identification and benchmarking.

C. Engineering of Dynamic Electrode−Electrolyte Interfaces. The electrode−electrolyte interface is the crucial region where catalytic reactions directly compete with contaminant adsorption and fouling. Most current systems rely on static interface designs, such as stable oxides (e.g., $Ni(OH)_2/Co_3O_4$, $NiMoO_4$)[144,145] and phosphate layers (e.g., CoPi, $(Co, Fe)PO_4$)[146] that demonstrate structural stability in freshwater but cannot adapt to the temporally and spatially varying contaminant profiles encountered in real seawater. To overcome these limitations, next-generation systems should consider employing dynamic, stimuli-responsive interfaces that actively repel contaminants or modulate their local environment according to changes in potential, pH, or ion concentration. State-of-the-art examples include interfaces featuring responsive polymers,[147] switchable wettability,[148] or potential-controlled surface charge that enhance water molecule access while selectively excluding multivalent cations and organic foulants. These electrodes that engineer local pH and ionic strength gradients can suppress the precipitation of insoluble hydroxides such as $Ca(OH)_2$ and $Mg(OH)_2$, which commonly obstruct cathodes during seawater splitting. For example, recent work by Zhai *et al.* utilized stimulus-responsive poly(N-isopropyl acrylamide)-poly(acrylic acid) (PNIPAM-PAA) hydrogels as dynamic interface layers on gold-nanocluster-modified electrodes to impede contamination and ion movement, enabling reversible, switchable electrochemical responses to changes in temperature, pH, and salt concentration, thereby enhancing the controllability and adaptability of the electrocatalytic system.[147] A similar goal-oriented work by Hu *et al.* demonstrated that a V_2O_3 interfacial layer on low-loaded Pt nanoparticles supported on a Ni_3N catalyst regulated the local microenvironment during seawater electrolysis by sequestering OH^- ions, increasing local alkalinity, and repelling chloride and alkaline earth salts, thereby effectively mitigating contamination and catalyst poisoning.[149]

D. Spin and Magnetic Modulation under Influence of Contaminants. The impurities which commonly interfere during water or seawater splitting can significantly alter the spin polarization and orbital occupancy of the active sites, influencing the electron transfer kinetics and mechanism during the OER and HER.[150] In seawater splitting, due to the presence of multiple redox-active species and competing parallel reactions, it is very necessary to understand how the ionic impurities modify spin states and magnetic exchange interactions to provide a new handle for optimizing activity, stability, and selectivity along with suppression of ClER. Advanced magnetic and spectroscopic probes combined with computational modeling could open promising avenues for spin- and orbital-controlled electrocatalysis under realistic conditions.

AUTHOR INFORMATION

Corresponding Author

Jonas Baltrusaitis − *Department of Chemical and Biomolecular Engineering, Lehigh University, Bethlehem, Pennsylvania 18015, United States;* orcid.org/0000-0001-5634-955X; Phone: +1-610-758-6836; Email: job314@lehigh.edu

Authors

Sahanaz Parvin − *Department of Chemical and Biomolecular Engineering, Lehigh University, Bethlehem, Pennsylvania 18015, United States*

Emmanuel Aransiola − *Department of Chemical and Biomolecular Engineering, Lehigh University, Bethlehem, Pennsylvania 18015, United States;* orcid.org/0009-0008-2521-2057

Sonakshi Saini − *School of Materials Science & Engineering, Georgia Institute of Technology, Atlanta, Georgia 30332, United States*

Matthew T. McDowell − *School of Materials Science & Engineering, Georgia Institute of Technology, Atlanta, Georgia 30332, United States; George W. Woodruff School of Mechanical Engineering, Georgia Institute of Technology, Atlanta, Georgia 30332, United States;* orcid.org/0000-0001-5552-3456

Seunghoon Lee − *Chemical Sciences Division, Oak Ridge National Laboratory, Oak Ridge, Tennessee 37831, United States*

Juliane Weber − *Chemical Sciences Division, Oak Ridge National Laboratory, Oak Ridge, Tennessee 37831, United States;* orcid.org/0000-0001-7961-0220

Yiqing Wu − *Chemical Sciences Division, Oak Ridge National Laboratory, Oak Ridge, Tennessee 37831, United States*

Yuanyuan Li − *Chemical Sciences Division, Oak Ridge National Laboratory, Oak Ridge, Tennessee 37831, United States*

Chang Liu − *Chemical Sciences Division, Oak Ridge National Laboratory, Oak Ridge, Tennessee 37831, United States*

Zili Wu − *Chemical Sciences Division, Oak Ridge National Laboratory, Oak Ridge, Tennessee 37831, United States;* orcid.org/0000-0002-4468-3240

Complete contact information is available at: https://pubs.acs.org/10.1021/acselectrochem.5c00381

Notes

The authors declare no competing financial interest.

ACKNOWLEDGMENTS

This work was supported as part of the Center for Understanding and Controlling Accelerated and Gradual Evolution of Materials for Energy (UNCAGE-ME), an Energy Frontier Research Center funded by the U.S. Department of Energy, Office of Science, Office of Basic Energy Sciences, under Award DE-SC0012577.

REFERENCES

(1) Seh, Z. W.; Kibsgaard, J.; Dickens, C. F.; Chorkendorff, I.; Nørskov, J. K.; Jaramillo, T. F. Combining Theory and Experiment in Electrocatalysis: Insights into Materials Design. *Science* **2017**, *355* (6321), No. eaad4998.

(2) *Energy and AI: Energy-demand from AI*; IEA: Paris, 2025.
(3) Chaubey, R.; Sahu, S.; James, O. O.; Maity, S. A Review on Development of Industrial Processes and Emerging Techniques for Production of Hydrogen from Renewable and Sustainable Sources. *Renewable Sustainable Energy Rev.* **2013**, *23*, 443−462.
(4) Zheng, Y.; Jiao, Y.; Jaroniec, M.; Qiao, S. Z. Advancing the Electrochemistry of the Hydrogen-Evolution Reaction through Combining Experiment and Theory. *Angew. Chem., Int. Ed.* **2015**, *54* (1), 52−65.
(5) Byers, E. A.; Hall, J. W.; Amezaga, J. M. Electricity Generation and Cooling Water Use: UK Pathways to 2050. *Global Environ. Change* **2014**, *25*, 16−30.
(6) Kumar, M.; Meena, B.; Subramanyam, P.; Suryakala, D.; Subrahmanyam, C. Recent Trends in Photoelectrochemical Water Splitting: The Role of Cocatalysts. *NPG Asia Mater.* **2022**, *14* (1), No. 88.
(7) Sapountzi, F. M.; Gracia, J. M.; Weststrate, C. J.; Fredriksson, H. O. A.; Niemantsverdriet, J. W. Electrocatalysts for the Generation of Hydrogen, Oxygen and Synthesis Gas. *Prog. Energy Combust. Sci.* **2017**, *58*, 1−35.
(8) Xian, F.; Miyatake, K.; Guo, L.; Shi, G.; Liu, F.; Mahmoud, A. M. A.; Yadav, V.; Wong, C. Y. Boosting the hydrogen-evolution reaction catalytic activity of Pt/C via well-designed anion-exchange ionomers. *Chem. Commun.* **2025**, *61*, 9412−9415.
(9) Guo, Y.; Park, T.; Yi, J. W.; Henzie, J.; Kim, J.; Wang, Z.; Jiang, B.; Bando, Y.; Sugahara, Y.; Tang, J.; Yamauchi, Y. Nanoarchitectonics for Transition-Metal-Sulfide-Based Electrocatalysts for Water Splitting. *Adv. Mater.* **2019**, *31* (17), No. 1807134.
(10) Yu, F.; Zhou, H.; Huang, Y.; Sun, J.; Qin, F.; Bao, J.; Goddard, W. A.; Chen, S.; Ren, Z. High-Performance Bifunctional Porous Non-Noble Metal Phosphide Catalyst for Overall Water Splitting. *Nat. Commun.* **2018**, *9* (1), No. 2551.
(11) Zhang, Y.; Ouyang, B.; Xu, J.; Jia, G.; Chen, S.; Rawat, R. S.; Fan, H. J. Rapid Synthesis of Cobalt Nitride Nanowires: Highly Efficient and Low-Cost Catalysts for Oxygen Evolution. *Angew. Chem., Int. Ed.* **2016**, *55* (30), 8670−8674.
(12) Gupta, S.; Patel, M. K.; Miotello, A.; Patel, N. Metal Boride-Based Catalysts for Electrochemical Water-Splitting: A Review. *Adv. Funct. Mater.* **2020**, *30* (1), No. 1906481.
(13) Zhou, H.; Yu, F.; Huang, Y.; Sun, J.; Zhu, Z.; Nielsen, R. J.; He, R.; Bao, J.; Goddard, W. A., III; Chen, S.; Ren, Z. Efficient Hydrogen Evolution by Ternary Molybdenum Sulfoselenide Particles on Self-Standing Porous Nickel Diselenide Foam. *Nat. Commun.* **2016**, *7* (1), No. 12765.
(14) Samira, S.; Hong, J.; Camayang, J. C. A.; Sun, K.; Hoffman, A. S.; Bare, S. R.; Nikolla, E. Dynamic Surface Reconstruction Unifies the Electrocatalytic Oxygen Evolution Performance of Nonstoichiometric Mixed Metal Oxides. *JACS Au* **2021**, *1* (12), 2224−2241.
(15) Parvin, S.; Bothra, N.; Dutta, S.; Maji, M.; Mura, M.; Kumar, A.; Chaudhary, D. K.; Rajput, P.; Kumar, M.; Pati, S. K.; Bhattacharyya, S. Inverse 'Intra-Lattice' Charge Transfer in Nickel-Molybdenum Dual Electrocatalysts Regulated by under-Coordinating the Molybdenum Center. *Chem. Sci.* **2023**, *14* (11), 3056−3069.
(16) Yuan, H.; Wang, S.; Ma, Z.; Kundu, M.; Tang, B.; Li, J.; Wang, X. Oxygen Vacancies Engineered Self-Supported B-Doped Co_3O_4 Nanowires as an Efficient Multifunctional Catalyst for Electrochemical Water Splitting and Hydrolysis of Sodium Borohydride. *Chem. Eng. J.* **2021**, *404*, No. 126474.
(17) Zhang, B.; Shan, J.; Wang, W.; Tsiakaras, P.; Li, Y. Oxygen Vacancy and Core-Shell Heterojunction Engineering of Anemone-Like CoP@CoOOH Bifunctional Electrocatalyst for Efficient Overall Water Splitting. *Small* **2022**, *18* (12), No. 2106012.
(18) Zhai, P.; Zhang, Y.; Wu, Y.; Gao, J.; Zhang, B.; Cao, S.; Zhang, Y.; Li, Z.; Sun, L.; Hou, J. Engineering Active Sites on Hierarchical Transition Bimetal Oxides/Sulfides Heterostructure Array Enabling Robust Overall Water Splitting. *Nat. Commun.* **2020**, *11* (1), No. 5462.
(19) Karak, S.; Koner, K.; Karmakar, A.; Mohata, S.; Nishiyama, Y.; Duong, N. T.; Thomas, N.; Ajithkumar, T. G.; Hossain, M. S.; Bandyopadhyay, S.; Kundu, S.; Banerjee, R. Morphology Tuning via Linker Modulation: Metal-Free Covalent Organic Nanostructures with Exceptional Chemical Stability for Electrocatalytic Water Splitting. *Adv. Mater.* **2024**, *36* (12), No. 2209919.
(20) Li, J.; Sun, J.; Li, Z.; Meng, X. Recent Advances in Electrocatalysts for Seawater Splitting in Hydrogen Evolution Reaction. *Int. J. Hydrogen Energy* **2022**, *47* (69), 29685−29697.
(21) Tong, W.; Forster, M.; Dionigi, F.; Dresp, S.; Erami, R. S.; Strasser, P.; Cowan, A. J.; Farràs, P. Electrolysis of Low-Grade and Saline Surface Water. *Nat. Energy* **2020**, *5* (5), 367−377.
(22) Wu, L.; Yu, L.; Zhang, F.; McElhenny, B.; Luo, D.; Karim, A.; Chen, S.; Ren, Z. Heterogeneous Bimetallic Phosphide Ni_2P-Fe_2P as an Efficient Bifunctional Catalyst for Water/Seawater Splitting. *Adv. Funct. Mater.* **2021**, *31* (1), No. 2006484.
(23) Zhou, Y.; Shen, Y.; Li, H. Effects of Metallic Impurities in Alkaline Electrolytes on Electro-Oxidation of Water and Alcohol Molecules. *J. Electrochem. Soc.* **2021**, *168* (12), No. 124516.
(24) Twight, L.; Tonsberg, A.; Samira, S.; Velinkar, K.; Dumpert, K.; Ou, Y.; Wang, L.; Nikolla, E.; Boettcher, S. W. Trace Fe Activates Perovskite Nickelate OER Catalysts in Alkaline Media via Redox-Active Surface Ni Species Formed during Electrocatalysis. *J. Catal.* **2024**, *432*, No. 115443.
(25) Tiwari, A.; Maagaard, T.; Chorkendorff, I.; Horch, S. Effect of Dissolved Glassware on the Structure-Sensitive Part of the Cu(111) Voltammogram in KOH. *ACS Energy Lett.* **2019**, *4* (7), 1645−1649.
(26) Becker, H.; Murawski, J.; Shinde, D. V.; Stephens, I. E. L.; Hinds, G.; Smith, G. Impact of Impurities on Water Electrolysis: A Review. *Sustainable Energy Fuels* **2023**, *7* (7), 1565−1603.
(27) Li, H.; Zhang, Y.; Chen, Y.; Li, Y.; Li, Z.; Yang, B.; Zhang, Q.; Lu, J.; Lei, L.; Xu, Z. J.; Hou, Y. Leveraging Iron in the Electrolyte to Improve Oxygen Evolution Reaction Performance: Fundamentals, Strategies, and Perspectives. *Angew. Chem., Int. Ed.* **2025**, *64* (8), No. e202423071.
(28) Spanos, I.; Masa, J.; Zeradjanin, A.; Schlögl, R. The Effect of Iron Impurities on Transition Metal Catalysts for the Oxygen Evolution Reaction in Alkaline Environment: Activity Mediators or Active Sites? *Catal. Lett.* **2021**, *151* (7), 1843−1856.
(29) Perumal, S.; Pokhrel, I.; Muhammad, U.; Shao, X.; Han, Y.; Kim, M.; Lee, H. Recent Advances in Electrochemical Water Splitting Electrocatalysts: Categorization by Parameters and Catalyst Types. *ACS Mater. Lett.* **2024**, *6* (8), 3625−3666.
(30) Kelly, N. A. Hydrogen Production by Water Electrolysis. In *Advances in Hydrogen Production, Storage and Distribution*; Basile, A., Iulianelli, A., Eds.; Elsevier: Amsterdam, 2014; pp 159−185.
(31) Xiang, C.; Papadantonakis, K. M.; Lewis, N. S. Principles and Implementations of Electrolysis Systems for Water Splitting. *Mater. Horiz.* **2016**, *3* (3), 169−173.
(32) Skúlason, E.; Tripkovic, V.; Björketun, M. E.; Gudmundsdóttir, S.; Karlberg, G.; Rossmeisl, J.; Bligaard, T.; Jónsson, H.; Nørskov, J. K. Modeling the Electrochemical Hydrogen Oxidation and Evolution Reactions on the Basis of Density Functional Theory Calculations. *J. Phys. Chem. C* **2010**, *114* (42), 18182−18197.
(33) Qadeer, M. A.; Zhang, X.; Farid, M. A.; Tanveer, M.; Yan, Y.; Du, S.; Huang, Z.-F.; Tahir, M.; Zou, J.-J. A Review on Fundamentals for Designing Hydrogen Evolution Electrocatalyst. *J. Power Sources* **2024**, *613*, No. 234856.
(34) Man, I. C.; Su, H.; Calle-Vallejo, F.; Hansen, H. A.; Martínez, J. I.; Inoglu, N. G.; Kitchin, J.; Jaramillo, T. F.; Nørskov, J. K.; Rossmeisl, J. Universality in Oxygen Evolution Electrocatalysis on Oxide Surfaces. *ChemCatChem* **2011**, *3* (7), 1159−1165.
(35) Appel, A. M.; Helm, M. L. Determining the Overpotential for a Molecular Electrocatalyst. *ACS Catal.* **2014**, *4* (2), 630−633.
(36) Coridan, R. H.; Nielander, A. C.; Francis, S. A.; McDowell, M. T.; Dix, V.; Chatman, S. M.; Lewis, N. S. Methods for Comparing the Performance of Energy-Conversion Systems for Use in Solar Fuels and Solar Electricity Generation. *Energy Environ. Sci.* **2015**, *8* (10), 2886−2901.
(37) Gong, S.; Meng, Y.; Jin, Z.; Hsu, H.-Y.; Du, M.; Liu, F. Recent Progress on the Stability of Electrocatalysts under High Current

https://doi.org/10.1021/acselectrochem.5c00381
ACS Electrochem. 2026, 2, 43−67

Densities toward Industrial Water Splitting. *ACS Catal.* **2024**, *14* (19), 14399−14435.
(38) Zhou, H.; Yu, F.; Zhu, Q.; Sun, J.; Qin, F.; Yu, L.; Bao, J.; Yu, Y.; Chen, S.; Ren, Z. Water Splitting by Electrolysis at High Current Densities under 1.6 Volts. *Energy Environ. Sci.* **2018**, *11* (10), 2858−2864.
(39) Shi, Y.; Du, W.; Zhou, W.; Wang, C.; Lu, S.; Lu, S.; Zhang, B. Unveiling the Promotion of Surface-Adsorbed Chalcogenate on the Electrocatalytic Oxygen Evolution Reaction. *Angew. Chem., Int. Ed.* **2020**, *59* (50), 22470−22474.
(40) Anantharaj, S.; Kundu, S. Do the Evaluation Parameters Reflect Intrinsic Activity of Electrocatalysts in Electrochemical Water Splitting? *ACS Energy Lett.* **2019**, *4* (6), 1260−1264.
(41) Bard, A. J.; Faulkner, L. R. *Electrochemical Methods: Fundamentals and Applications*, 2nd ed.; Wiley, 2001.
(42) Anantharaj, S.; Karthik, P. E.; Noda, S. The Significance of Properly Reporting Turnover Frequency in Electrocatalysis Research. *Angew. Chem., Int. Ed.* **2021**, *60* (43), 23051−23067.
(43) Kempler, P. A.; Nielander, A. C. Reliable Reporting of Faradaic Efficiencies for Electrocatalysis Research. *Nat. Commun.* **2023**, *14* (1), No. 1158.
(44) Akbayrak, M.; Önal, A. M. High Durability and Electrocatalytic Activity Toward Hydrogen Evolution Reaction with Ultralow Rhodium Loading on Titania. *J. Electrochem. Soc.* **2020**, *167* (15), No. 156501.
(45) Liu, W.; Hu, E.; Jiang, H.; Xiang, Y.; Weng, Z.; Li, M.; Fan, Q.; Yu, X.; Altman, E. I.; Wang, H. A Highly Active and Stable Hydrogen Evolution Catalyst Based on Pyrite-Structured Cobalt Phosphosulfide. *Nat. Commun.* **2016**, *7* (1), No. 10771.
(46) Asiri, A. M.; Adeosun, W. A.; Khan, S. B.; Alamry, K. A.; Marwani, H. M.; Zakeeruddin, S. M.; Grätzel, M. Solid-State Synthesis of $CdFe_2O_4$ Binary Catalyst for Potential Application in Renewable Hydrogen Fuel Generation. *Sci. Rep.* **2022**, *12* (1), No. 1632.
(47) Li, Y.-W.; Zhang, W.-J.; Li, J.; Ma, H.-Y.; Du, H.-M.; Li, D.-C.; Wang, S.-N.; Zhao, J.-S.; Dou, J.-M.; Xu, L. Fe-MOF-Derived Efficient ORR/OER Bifunctional Electrocatalyst for Rechargeable Zinc-Air Batteries. *ACS Appl. Mater. Interfaces* **2020**, *12* (40), 44710−44719.
(48) Du, Z.; Zhao, H.; Yi, S.; Xia, Q.; Gong, Y.; Zhang, Y.; Cheng, X.; Li, Y.; Gu, L.; Świerczek, K. High-Performance Anode Material $Sr_2FeMo_{0.65}Ni_{0.35}O_{6-\delta}$ with *In Situ* Exsolved Nanoparticle Catalyst. *ACS Nano* **2016**, *10* (9), 8660−8669.
(49) Meng, Y.; Zhang, X.; Hung, W.-H.; He, J.; Tsai, Y.-S.; Kuang, Y.; Kenney, M. J.; Shyue, J.-J.; Liu, Y.; Stone, K. H.; Zheng, X.; Suib, S. L.; Lin, M.-C.; Liang, Y.; Dai, H. Highly Active Oxygen Evolution Integrated with Efficient CO_2 to CO Electroreduction. *Proc. Natl. Acad. Sci. U.S.A.* **2019**, *116* (48), 23915−23922.
(50) Maji, M.; Dutta, S.; Jena, R.; Dey, A.; Maji, T. K.; Pati, S. K.; Bhattacharyya, S. Hydrogen Evolution in Neutral Media by Differential Intermediate Binding at Charge-Modulated Sites of a Bimetallic Alloy Electrocatalyst. *Angew. Chem., Int. Ed.* **2024**, *63* (22), No. e202403697.
(51) Zhang, B.; Zheng, X.; Voznyy, O.; Comin, R.; Bajdich, M.; García-Melchor, M.; Han, L.; Xu, J.; Liu, M.; Zheng, L.; García De Arquer, F. P.; Dinh, C. T.; Fan, F.; Yuan, M.; Yassitepe, E.; Chen, N.; Regier, T.; Liu, P.; Li, Y.; De Luna, P.; Janmohamed, A.; Xin, H. L.; Yang, H.; Vojvodic, A.; Sargent, E. H. Homogeneously Dispersed Multimetal Oxygen-Evolving Catalysts. *Science* **2016**, *352* (6283), 333−337.
(52) Trasatti, S. Electrocatalysis by Oxides—Attempt at a Unifying Approach. *J. Electroanal. Chem. Interfacial Electrochem.* **1980**, *111* (1), 125−131.
(53) Song, Q.; Li, J.; Zhang, B.; Li, H.; Liu, X. Controlling the D-Band for Improved Oxygen Evolution Performance in Ni-Modulated Ultrafine Co Nanoparticles Embedded in Nitrogen-Doped Carbon Microspheres. *J. Colloid Interface Sci.* **2022**, *623*, 44−53.
(54) Li, X.; Liu, J.; Cai, Q.; Kan, Z.; Liu, S.; Zhao, J. Engineering d-Band Center of Iron Single Atom Site through Boron Incorporation to Trigger the Efficient Bifunctional Oxygen Electrocatalysis. *J. Colloid Interface Sci.* **2022**, *628*, 331−342.
(55) Wang, R.; Zhong, J.; Li, D.; Meng, J.; Huang, W.; Ma, X.; Guo, W.; Tian, F.; Li, C. Engineering D-Band Center of Cobalt Active Sites via Dual Coordination with Nitrogen-Doped Carbon Nanotube and $Ti_3C_2T_x$ MXene toward Electrocatalytic Oxygen Reduction for H_2O_2 Production. *Chem. Eng. J.* **2024**, *488*, No. 150894.
(56) Jiang, J.; Sun, F.; Zhou, S.; Hu, W.; Zhang, H.; Dong, J.; Jiang, Z.; Zhao, J.; Li, J.; Yan, W.; Wang, M. Atomic-Level Insight into Super-Efficient Electrocatalytic Oxygen Evolution on Iron and Vanadium Co-Doped Nickel (Oxy)hydroxide. *Nat. Commun.* **2018**, *9*, No. 2885.
(57) Kozawa, A. Effects of Anions and Cations on Oxygen Reduction and Oxygen Evolution Reactions on Platinum Electrodes. *J. Electroanal. Chem. (1959)* **1964**, *8* (1), 20−39.
(58) Klaus, S.; Cai, Y.; Louie, M. W.; Trotochaud, L.; Bell, A. T. Effects of Fe Electrolyte Impurities on $Ni(OH)_2$/NiOOH Structure and Oxygen Evolution Activity. *J. Phys. Chem. C* **2015**, *119* (13), 7243−7254.
(59) Vij, V.; Sultan, S.; Harzandi, A. M.; Meena, A.; Tiwari, J. N.; Lee, W.-G.; Yoon, T.; Kim, K. S. Nickel-Based Electrocatalysts for Energy-Related Applications: Oxygen Reduction, Oxygen Evolution, and Hydrogen Evolution Reactions. *ACS Catal.* **2017**, *7* (10), 7196−7225.
(60) Gao, M.; Sheng, W.; Zhuang, Z.; Fang, Q.; Gu, S.; Jiang, J.; Yan, Y. Efficient Water Oxidation Using Nanostructured α-Nickel-Hydroxide as an Electrocatalyst. *J. Am. Chem. Soc.* **2014**, *136* (19), 7077−7084.
(61) Spanos, I.; Tesch, M. F.; Yu, M.; Tüysüz, H.; Zhang, J.; Feng, X.; Müllen, K.; Schlögl, R.; Mechler, A. K. Facile Protocol for Alkaline Electrolyte Purification and Its Influence on a Ni-Co Oxide Catalyst for the Oxygen Evolution Reaction. *ACS Catal.* **2019**, *9* (9), 8165−8170.
(62) Trotochaud, L.; Young, S. L.; Ranney, J. K.; Boettcher, S. W. Nickel-Iron Oxyhydroxide Oxygen-Evolution Electrocatalysts: The Role of Intentional and Incidental Iron Incorporation. *J. Am. Chem. Soc.* **2014**, *136* (18), 6744−6753.
(63) Singh, R. N.; Pandey, J. P.; Anitha, K. L. Preparation of Electrodeposited Thin Films of Nickel-Iron Alloys on Mild Steel for Alkaline Water Electrolysis. Part I: Studies on Oxygen Evolution. *Int. J. Hydrogen Energy* **1993**, *18*, 467−473.
(64) Lopes, P. P.; Chung, D. Y.; Rui, X.; Zheng, H.; He, H.; Farinazzo Bergamo Dias Martins, P.; Strmcnik, D.; Stamenkovic, V. R.; Zapol, P.; Mitchell, J. F.; Klie, R. F.; Markovic, N. M. Dynamically Stable Active Sites from Surface Evolution of Perovskite Materials during the Oxygen Evolution Reaction. *J. Am. Chem. Soc.* **2021**, *143* (7), 2741−2750.
(65) Yu, X.; Xu, S.; Liu, X.; Cheng, X.; Du, Y.; Wu, Q. Mn-Doped $NiCo_2S_4$ Nanosheet Array as an Efficient and Durable Electrocatalyst for Oxygen Evolution Reaction. *J. Alloys Compd.* **2021**, *878*, No. 160388.
(66) Li, J.; Zhou, W.; Huang, Y.; Xie, L.; Wang, J.; Li, J.; Meng, X.; Gao, J. Cobalt-Doped Ultrathin $Ni(OH)_2$ Nanosheet Array @NiCo Alloy toward an Efficient Oxygen Evolution Reaction and the Electrooxidation of Phenoxyethanol. *Energy Fuels* **2024**, *38* (1), 617−627.
(67) Hong, W. T.; Welsch, R. E.; Shao-Horn, Y. Descriptors of Oxygen-Evolution Activity for Oxides: A Statistical Evaluation. *J. Phys. Chem. C* **2016**, *120* (1), 78−86.
(68) Bockris, J. O.; Otagawa, T. The Electrocatalysis of Oxygen Evolution on Perovskites. *J. Electrochem. Soc.* **1984**, *131* (2), 290−302.
(69) Naderi, A.; Jourshabani, M.; Lee, B.-K. Effects of D-Block Transition Metal Impurities on a Carbon Cloth/$Ni(OH)_2$ Interface for Electrocatalytic Oxygen Evolution Reaction. *ACS Sustainable Chem. Eng.* **2023**, *11* (24), 9010−9019.
(70) Pham, T. H. M.; Shen, T.-H.; Ko, Y.; Zhong, L.; Lombardo, L.; Luo, W.; Horike, S.; Tileli, V.; Züttel, A. Elucidating the Mechanism of Fe Incorporation in In Situ Synthesized Co−Fe Oxygen-Evolving Nanocatalysts. *J. Am. Chem. Soc.* **2023**, *145* (43), 23691−23701.
(71) Li, Y.; Liu, J.; Li, S.; Peng, S. Codecoration of Phosphate and Iron for Improving Oxygen Evolution Reaction of Layered $Ni(OH)_2$/NiOOH. *ACS Catal.* **2024**, *14* (7), 4807−4819.
(72) Liang, R.; Zhang, B.; Du, Y.; Han, X.; Li, S.; Xu, P. Understanding the Anion Effect of Basic Cobalt Salts for the Electrocatalytic Oxygen Evolution Reaction. *ACS Catal.* **2023**, *13* (13), 8821−8829.
(73) Li, Z.; Xue, K.-H.; Wang, J.; Li, J.-G.; Ao, X.; Sun, H.; Song, X.; Lei, W.; Cao, Y.; Wang, C. Cation and Anion Co-Doped Perovskite

Nanofibers for Highly Efficient Electrocatalytic Oxygen Evolution. *ACS Appl. Mater. Interfaces* **2020**, *12* (37), 41259−41268.
(74) Xi, B.; Wu, B.; Duan, Z.; Zhang, T.; Lyu, S.; Zheng, S.; Zhao, Y.; Lei, C. Modulating the Electronic Structure of NiFe Layered Double Hydroxide via Anion Engineering for Enhanced Oxygen Evolution. *J. Colloid Interface Sci.* **2025**, *689*, No. 137258.
(75) Kamat, G. A.; Zamora Zeledón, J. A.; Gunasooriya, G. T. K. K.; Dull, S. M.; Perryman, J. T.; Nørskov, J. K.; Stevens, M. B.; Jaramillo, T. F. Acid Anion Electrolyte Effects on Platinum for Oxygen and Hydrogen Electrocatalysis. *Commun. Chem.* **2022**, *5* (1), No. 20.
(76) Gao, R.; Li, G.-D.; Hu, J.; Wu, Y.; Lian, X.; Wang, D.; Zou, X. In Situ Electrochemical Formation of NiSe/NiO_x Core/Shell Nano-Electrocatalysts for Superior Oxygen Evolution Activity. *Catal. Sci. Technol.* **2016**, *6* (23), 8268−8275.
(77) Monteiro, M. C. O.; Goyal, A.; Moerland, P.; Koper, M. T. M. Understanding Cation Trends for Hydrogen Evolution on Platinum and Gold Electrodes in Alkaline Media. *ACS Catal.* **2021**, *11* (23), 14328−14335.
(78) Xue, S.; Garlyyev, B.; Watzele, S.; Liang, Y.; Fichtner, J.; Pohl, M. D.; Bandarenka, A. S. Influence of Alkali Metal Cations on the Hydrogen Evolution Reaction Activity of Pt, Ir, Au, and Ag Electrodes in Alkaline Electrolytes. *ChemElectroChem* **2018**, *5* (17), 2326−2329.
(79) Trasatti, S. Work Function, Electronegativity, and Electrochemical Behaviour of Metals. III. Electrolytic Hydrogen Evolution in Acid Solutions. *J. Electroanal. Chem. Interfacial Electrochem.* **1972**, *39* (1), 163−184.
(80) Kötz, E. R.; Stucki, S. Ruthenium Dioxide as a Hydrogen-Evolving Cathode. *J. Appl. Electrochem.* **1987**, *17* (6), 1190−1197.
(81) Saini, S.; Wright, S. C.; Parvin, S.; Baltrusaitis, J.; McDowell, M. T. Investigating the Effects of Copper Impurity Deposition on the Structure and Electrochemical Behavior of Hydrogen Evolution Electrocatalyst Materials. *ACS Appl. Energy Mater.* **2025**, *8* (2), 1143−1153.
(82) Nidola, A.; Schira, R. Poisoning Mechanisms and Structural Analyses on Metallic Contaminated Cathode Catalysts in Chlor-Alkali Membrane Cell Technology. *J. Electrochem. Soc.* **1986**, *133* (8), 1653−1656.
(83) Woldu, A. R.; Huang, Z.; Zhao, P.; Hu, L.; Astruc, D. Electrochemical CO_2 Reduction (CO_2RR) to Multi-Carbon Products over Copper-Based Catalysts. *Coord. Chem. Rev.* **2022**, *454*, No. 214340.
(84) Nitopi, S.; Bertheussen, E.; Scott, S. B.; Liu, X.; Engstfeld, A. K.; Horch, S.; Seger, B.; Stephens, I. E. L.; Chan, K.; Hahn, C.; Nørskov, J. K.; Jaramillo, T. F.; Chorkendorff, I. Progress and Perspectives of Electrochemical CO_2 Reduction on Copper in Aqueous Electrolyte. *Chem. Rev.* **2019**, *119* (12), 7610−7672.
(85) Li, X.; Gunathunge, C. M.; Agrawal, N.; Montalvo-Castro, H.; Jin, J.; Janik, M. J.; Waegele, M. M. Impact of Alkali Metal Cations and Iron Impurities on the Evolution of Hydrogen on Cu Electrodes in Alkaline Electrolytes. *J. Electrochem. Soc.* **2020**, *167* (10), No. 106505.
(86) Wang, Z.; Xu, W.; Yu, K.; Feng, Y.; Zhu, Z. 2D Heterogeneous Vanadium Compound Interfacial Modulation Enhanced Synergistic Catalytic Hydrogen Evolution for Full pH Range Seawater Splitting. *Nanoscale* **2020**, *12* (10), 6176−6187.
(87) Wu, X.; Zhou, S.; Wang, Z.; Liu, J.; Pei, W.; Yang, P.; Zhao, J.; Qiu, J. Engineering Multifunctional Collaborative Catalytic Interface Enabling Efficient Hydrogen Evolution in All pH Range and Seawater. *Adv. Energy Mater.* **2019**, *9* (34), No. 1901333.
(88) Lv, Q.; Han, J.; Tan, X.; Wang, W.; Cao, L.; Dong, B. Featherlike NiCoP Holey Nanoarrys for Efficient and Stable Seawater Splitting. *ACS Appl. Energy Mater.* **2019**, *2* (5), 3910−3917.
(89) Yu, L.; Zhu, Q.; Song, S.; McElhenny, B.; Wang, D.; Wu, C.; Qin, Z.; Bao, J.; Yu, Y.; Chen, S.; Ren, Z. Non-Noble Metal-Nitride Based Electrocatalysts for High-Performance Alkaline Seawater Electrolysis. *Nat. Commun.* **2019**, *10* (1), No. 5106.
(90) Debnath, B.; Parvin, S.; Dixit, H.; Bhattacharyya, S. Oxygen-Defect-Rich Cobalt Ferrite Nanoparticles for Practical Water Electrolysis with High Activity and Durability. *ChemSusChem* **2020**, *13* (15), 3875−3886.
(91) Fan, R.; Liu, C.; Li, Z.; Huang, H.; Feng, J.; Li, Z.; Zou, Z. Ultrastable Electrocatalytic Seawater Splitting at Ampere-Level Current Density. *Nat. Sustain.* **2024**, *7* (2), 158−167.
(92) Dresp, S.; Dionigi, F.; Klingenhof, M.; Strasser, P. Direct Electrolytic Splitting of Seawater: Opportunities and Challenges. *ACS Energy Lett.* **2019**, *4* (4), 933−942.
(93) Xu, X.; Lu, Y.; Shi, J.; Hao, X.; Ma, Z.; Yang, K.; Zhang, T.; Li, C.; Zhang, D.; Huang, X.; He, Y. Corrosion-Resistant Cobalt Phosphide Electrocatalysts for Salinity Tolerance Hydrogen Evolution. *Nat. Commun.* **2023**, *14* (1), No. 7708.
(94) Niu, X.; Tang, Q.; He, B.; Yang, P. Robust and Stable Ruthenium Alloy Electrocatalysts for Hydrogen Evolution by Seawater Splitting. *Electrochim. Acta* **2016**, *208*, 180−187.
(95) Kuhn, A. T.; Chan, C. Y. pH Changes at Near-Electrode Surfaces. *J. Appl. Electrochem.* **1983**, *13* (2), 189−207.
(96) Kirk, D. W.; Ledas, A. E. Precipitate Formation during Sea Water Electrolysis. *Int. J. Hydrogen Energy* **1982**, *7* (12), 925−932.
(97) Jin, H.; Xu, J.; Liu, H.; Shen, H.; Yu, H.; Jaroniec, M.; Zheng, Y.; Qiao, S.-Z. Emerging Materials and Technologies for Electrocatalytic Seawater Splitting. *Sci. Adv.* **2023**, *9* (42), No. eadi7755.
(98) Jin, H.; Liu, X.; Vasileff, A.; Jiao, Y.; Zhao, Y.; Zheng, Y.; Qiao, S.-Z. Single-Crystal Nitrogen-Rich Two-Dimensional Mo_5N_6 Nanosheets for Efficient and Stable Seawater Splitting. *ACS Nano* **2018**, *12* (12), 12761−12769.
(99) Guo, J.; Zheng, Y.; Hu, Z.; Zheng, C.; Mao, J.; Du, K.; Jaroniec, M.; Qiao, S.-Z.; Ling, T. Direct Seawater Electrolysis by Adjusting the Local Reaction Environment of a Catalyst. *Nat. Energy* **2023**, *8* (3), 264−272.
(100) Exner, K. S. Controlling Stability and Selectivity in the Competing Chlorine and Oxygen Evolution Reaction over Transition Metal Oxide Electrodes. *ChemElectroChem* **2019**, *6* (13), 3401−3409.
(101) Vos, J. G.; Liu, Z.; Speck, F. D.; Perini, N.; Fu, W.; Cherevko, S.; Koper, M. T. M. Selectivity Trends Between Oxygen Evolution and Chlorine Evolution on Iridium-Based Double Perovskites in Acidic Media. *ACS Catal.* **2019**, *9* (9), 8561−8574.
(102) Zeradjanin, A. R.; Menzel, N.; Schuhmann, W.; Strasser, P. On the Faradaic Selectivity and the Role of Surface Inhomogeneity during the Chlorine Evolution Reaction on Ternary Ti-Ru-Ir Mixed Metal Oxide Electrocatalysts. *Phys. Chem. Chem. Phys.* **2014**, *16* (27), 13741−13747.
(103) Sohrabnejad-Eskan, I.; Goryachev, A.; Exner, K. S.; Kibler, L. A.; Hensen, E. J. M.; Hofmann, J. P.; Over, H. Temperature-Dependent Kinetic Studies of the Chlorine Evolution Reaction over RuO_2 (110) Model Electrodes. *ACS Catal.* **2017**, *7* (4), 2403−2411.
(104) Vos, J. G.; Wezendonk, T. A.; Jeremiasse, A. W.; Koper, M. T. M. MnO_x/IrO_x as Selective Oxygen Evolution Electrocatalyst in Acidic Chloride Solution. *J. Am. Chem. Soc.* **2018**, *140* (32), 10270−10281.
(105) Li, J.; Liu, Y.; Chen, H.; Zhang, Z.; Zou, X. Design of a Multilayered Oxygen-Evolution Electrode with High Catalytic Activity and Corrosion Resistance for Saline Water Splitting. *Adv. Funct. Mater.* **2021**, *31* (27), No. 2101820.
(106) Tan, L.; Yu, J.; Wang, C.; Wang, H.; Liu, X.; Gao, H.; Xin, L.; Liu, D.; Hou, W.; Zhan, T. Partial Sulfidation Strategy to NiFe-LDH@$FeNi_2S_4$ Heterostructure Enable High-Performance Water/Seawater Oxidation. *Adv. Funct. Mater.* **2022**, *32* (29), No. 2200951.
(107) Schott, C. M.; Schneider, P. M.; Song, K.-T.; Yu, H.; Götz, R.; Haimerl, F.; Gubanova, E.; Zhou, J.; Schmidt, T. O.; Zhang, Q.; Alexandrov, V.; Bandarenka, A. S. How to Assess and Predict Electrical Double Layer Properties. Implications for Electrocatalysis. *Chem. Rev.* **2024**, *124* (22), 12391−12462.
(108) Roger, I.; Symes, M. D. Silver Leakage from Ag/AgCl Reference Electrodes as a Potential Cause of Interference in the Electrocatalytic Hydrogen Evolution Reaction. *ACS Appl. Mater. Interfaces* **2017**, *9* (1), 472−478.
(109) Chen, R.; Yang, C.; Cai, W.; Wang, H.-Y.; Miao, J.; Zhang, L.; Chen, S.; Liu, B. Use of Platinum as the Counter Electrode to Study the Activity of Nonprecious Metal Catalysts for the Hydrogen Evolution Reaction. *ACS Energy Lett.* **2017**, *2* (5), 1070−1075.

https://doi.org/10.1021/acselectrochem.5c00381
ACS Electrochem. 2026, 2, 43−67

(110) Ota, K.-I.; Nishigori, S.; Kamiya, N. Dissolution of Platinum Anodes in Sulfuric Acid Solution. *J. Electroanal. Chem. Interfacial Electrochem.* **1988**, *257* (1-2), 205−215.
(111) Wei, R.; Fang, M.; Dong, G.; Ho, J. C. Is Platinum a Suitable Counter Electrode Material for Electrochemical Hydrogen Evolution Reaction? *Sci. Bull.* **2017**, *62* (14), 971−973.
(112) Hasan, M. M.; Allam, N. K. An Alternative, Low-Dissolution Counter Electrode to Prevent Deceptive Enhancement of HER Overpotential. *Sci. Rep.* **2022**, *12* (1), No. 9368.
(113) Li, X.; Xu, S. L.; Li, J.; Zhang, S. S.; Zhang, B. Y.; Zhao, R. Da; Zhao, D. P.; Wu, F. F. NiFe-LDH as a Bifunctional Electrocatalyst for Efficient Water and Seawater Electrolysis: Enhanced Oxygen Evolution and Hydrogen Evolution Reactions. *Nanoscale. Adv.* **2025**, *7* (18), 5546−5560.
(114) Wijten, J. H. J.; Mandemaker, L. D. B.; Van Eeden, T. C.; Dubbeld, J. E.; Weckhuysen, B. M. In Situ Study on Ni-Mo Stability in a Water-Splitting Device: Effect of Catalyst Substrate and Electric Potential. *ChemSusChem* **2020**, *13* (12), 3172−3179.
(115) Colli, A. N.; Girault, H. H.; Battistel, A. Non-Precious Electrodes for Practical Alkaline Water Electrolysis. *Materials* **2019**, *12* (8), No. 1336.
(116) Chen, L.; Liang, M.; Wan, W.; Tang, J.; Lin, B.; Yang, X.; Chen, Y.; Chen, Y. Corrosion of Commercial Pure Titanium and Two Titanium Alloys in Extremely High-Chloride and High-Alkali Seawater Electrolysis Environment. *J. Alloys Compd.* **2025**, *1020*, No. 179431.
(117) Yang, L.-J.; Guan, H.-Y.; Yuan, S.; Sun, T.; Jiang, A.-N.; Feng, J.-J. Research Progress of Chlorine Corrosion Resistance in Seawater Electrolysis: Materials and Technologies. *Chem. Eng. J.* **2025**, *503*, No. 158458.
(118) Zhang, S.; Xu, W.; Zhu, J.; Wen, Y.; Wang, Y.; Dai, Y.; Chen, H.; Yi, L.; Tian, Z.; Lu, Z. Ni-X (X = Cl, Br) Reaction Energy Barrier Regulation in Passive Film for Stable Oxygen Evolution Reaction in Alkaline Seawater. *Adv. Mater.* **2025**, DOI: 10.1002/adma.202512787.
(119) Zhang, S.; Wang, Y.; Li, S.; Wang, Z.; Chen, H.; Yi, L.; Chen, X.; Yang, Q.; Xu, W.; Wang, A.; Lu, Z. Concerning the Stability of Seawater Electrolysis: A Corrosion Mechanism Study of Halide on Ni-Based Anode. *Nat. Commun.* **2023**, *14* (1), No. 4822.
(120) Sharkh, B. A.; Al-Amoudi, A. A.; Farooque, M.; Fellows, C. M.; Ihm, S.; Lee, S.; Li, S.; Voutchkov, N. Seawater Desalination Concentrate—A New Frontier for Sustainable Mining of Valuable Minerals. *npj Clean Water* **2022**, *5* (1), No. 9.
(121) Todolí, J. L.; Mermet, J. M. Sample Introduction Systems for the Analysis of Liquid Microsamples by ICP-AES and ICP-MS. *Spectrochim. Acta, Part B* **2006**, *61* (3), 239−283.
(122) Andrade, J. D. X-ray Photoelectron Spectroscopy (XPS). In *Surface and Interfacial Aspects of Biomedical Polymers*; Andrade, J. D., Ed.; Springer: Boston, MA, 1985; pp 105−195.
(123) Pelevin, I. A.; Kaminskaya, T. P.; Chernyshikhin, S. V.; Larionov, K. B.; Dzidziguri, E. L. Atomic Force Microscopy's Application for Surface Structure Investigation of Materials Synthesized by Laser Powder Bed Fusion. *Compounds* **2024**, *4* (3), 562−570.
(124) Egerton, R. F. *Electron Energy-Loss Spectroscopy in the Electron Microscope*, 3rd ed.; Springer: New York, 2011.
(125) Zhang, D.; Liu, X.; Zhao, Y.; Zhang, H.; Rudnev, A. V.; Li, J.-F. *In Situ* Raman Spectroscopic Studies of CO_2 Reduction Reactions: From Catalyst Surface Structures to Reaction Mechanisms. *Chem. Sci.* **2025**, *16* (12), 4916−4936.
(126) Chen, M.; Liu, D.; Qiao, L.; Zhou, P.; Feng, J.; Ng, K. W.; Liu, Q.; Wang, S.; Pan, H. In-Situ/Operando Raman Techniques for in-Depth Understanding on Electrocatalysis. *Chem. Eng. J.* **2023**, *461*, No. 141939.
(127) Scanning Beam Methods. In *Electron Microscopy: Principles and Fundamentals*; Amelinckx, S., Van Dyck, D., van Landuyt, J., van Tendeloo, G., Eds.; VCH, 1997; pp 305−497.
(128) Zhu, Y.; Xu, M.; Zhou, W. High-Resolution Electron Microscopy for Heterogeneous Catalysis Research. *Chin. Phys. B* **2018**, *27* (5), No. 056804.
(129) Gupta, S.; Bhattacharyya, S. Footprints of Scanning Probe Microscopy on Halide Perovskites. *Chem. Commun.* **2024**, *60* (82), 11685−11701.
(130) Krishna, D. N. G.; Philip, J. Review on Surface-Characterization Applications of X-ray Photoelectron Spectroscopy (XPS): Recent Developments and Challenges. *Appl. Surf. Sci. Adv.* **2022**, *12*, No. 100332.
(131) *Infrared and Raman Spectroscopy in Forensic Science*, 1st ed.; Chalmers, J. M., Edwards, H. G. M., Hargreaves, M. D., Eds.; Wiley, 2012.
(132) Browne, W. R.; McGarvey, J. J. The Raman Effect and Its Application to Electronic Spectroscopies in Metal-Centered Species: Techniques and Investigations in Ground and Excited States. *Coord. Chem. Rev.* **2007**, *251* (3-4), 454−473.
(133) Parvin, S.; Aransiola, E.; Ammar, M.; Lee, S.; Zhang, L.; Weber, J.; Baltrusaitis, J. Tailored $Ni(OH)_2$ /CuCo/$Ni(OH)_2$ Composite Interfaces for Efficient and Durable Urea Oxidation Reaction. *ACS Appl. Mater. Interfaces* **2024**, *16* (49), 67715−67729.
(134) Cheraparambil, H.; Vega-Paredes, M.; Wang, Y.; Tüysüz, H.; Scheu, C.; Weidenthaler, C. Deciphering the Role of Fe Impurities in the Electrolyte Boosting the OER Activity of $LaNiO_3$. *J. Mater. Chem. A* **2024**, *12* (9), 5194−5203.
(135) Qazi, H.; Chauhan, D.; Ahn, Y.-H. Impurity Impacts and Mitigation Strategies in Alkaline Seawater Electrolysis. *Int. J. Hydrogen Energy* **2025**, *99*, 155−164.
(136) Deng, R.; Zhang, B.; Zhang, Q. Electrochemical Water Splitting for Scale Hydrogen Production: From the Laboratory to Industrial Applications. *ChemCatChem* **2024**, *16* (14), No. e202301165.
(137) Dmitrieva, A. P.; Fomkina, A. S.; Tracey, C. T.; Romanenko, E. A.; Ayati, A.; Krivoshapkin, P. V.; Krivoshapkina, E. F. AI and ML for Selecting Viable Electrocatalysts: Progress and Perspectives. *J. Mater. Chem. A* **2024**, *12* (45), 31074−31102.
(138) Zhang, J.; Guo, C.; Fang, S.; Zhao, X.; Li, L.; Jiang, H.; Liu, Z.; Fan, Z.; Xu, W.; Xiao, J.; Zhong, M. Accelerating Electrochemical CO_2 Reduction to Multi-Carbon Products via Asymmetric Intermediate Binding at Confined Nanointerfaces. *Nat. Commun.* **2023**, *14* (1), No. 1298.
(139) Shehzad, A.; Yi, Q.; Cui, C.; Luo, Z. Electrocatalytic Nitrogen Reduction to Ammonia by Graphene-Supported Au_4Cu_2 and Au_2Ag_2 Nanoclusters. *Nanoscale* **2025**, *17* (12), 7453−7459.
(140) Liu, D.; Cai, Y.; Wang, X.; Zhuo, Y.; Sui, X.; Pan, H.; Wang, Z. Innovations in Electrocatalysts, Hybrid Anodic Oxidation, and Electrolyzers for Enhanced Direct Seawater Electrolysis. *Energy Environ. Sci.* **2024**, *17* (19), 6897−6942.
(141) Feng, Y.; Chen, Y.; Zheng, L.; Chen, X.; Li, T.; Zhao, W. Descriptors Construction and Application in Catalytic Site Design. *iScience* **2025**, *28* (8), No. 113080.
(142) Prajapati, A.; Hahn, C.; Weidinger, I. M.; Shi, Y.; Lee, Y.; Alexandrova, A. N.; Thompson, D.; Bare, S. R.; Chen, S.; Yan, S.; Kornienko, N. Best Practices for In-Situ and Operando Techniques within Electrocatalytic Systems. *Nat. Commun.* **2025**, *16* (1), No. 2593.
(143) Lim, A.; Ham, K.; Elrefaei, S.; Spanos, I. Operando Interpretation of Reaction Mechanisms and Local Phenomena on OER Catalysts in Seawater Electrolysis. *Curr. Opin. Electrochem* **2024**, *47*, No. 101560.
(144) Li, C.; Luo, X.; Wang, Y.; Zhu, M.; Li, D.; Guo, S.; Wang, W.; Xu, X. Industrial Alkaline Electrolyzers Enabled by Interface-Engineered Cobalt Oxide Electrodes for High-Efficiency Water Splitting. *Adv. Sci.* **2025**, *12* (35), No. e08013.
(145) Chueh, C. C.; Yu, S. E.; Wu, H. C.; Hsu, C. C.; Ni, I. C.; Wu, C. I.; Cheng, I. C.; Chen, J. Z. Enhanced Oxygen Evolution Reaction Performance of $NiMoO_4$/Carbon Paper Electrocatalysts in Anion Exchange Membrane Water Electrolysis by Atmospheric-Pressure Plasma Jet Treatment. *Langmuir* **2024**, *40* (46), 24675−24686.
(146) Rekha, P.; Yadav, S.; Singh, L. A Review on Cobalt Phosphate-Based Materials as Emerging Catalysts for Water Splitting. *Ceram. Int.* **2021**, *47* (12), 16385−16401.
(147) Zhai, Z.; Yang, C.; Kai, Y.; Li, J.; Meng, L.; Zhao, M.; Wang, Y.; Shi, K.; Yao, H. Construction of Intelligent Interfaces Based on

Stimulus-Responsive Hydrogels and Ligand-Free Gold Nanoparticles for Electrocatalysis of Isoquercitrin. *Surf. Interfaces* **2023**, *42*, No. 103436.
(148) Shen, T. H.; Spillane, L.; Peng, J.; Shao-Horn, Y.; Tileli, V. Switchable Wetting of Oxygen-Evolving Oxide Catalysts. *Nat. Catal.* **2022**, *5* (1), 30−36.
(149) Hu, H.; Zhang, Z.; Liu, L.; Che, X.; Wang, J.; Zhu, Y.; Attfield, J. P.; Yang, M. Efficient and Durable Seawater Electrolysis with a V_2O_3 -Protected Catalyst. *Sci. Adv.* **2024**, *10* (20), No. eadn7012.
(150) Parvin, S.; Bhattacharyya, S. Electrocatalysis at Quantum Edge: Role of Spin, Orbital, and Magnetic Interactions. *ACS Appl. Energy Mater.* **2025**, *8* (20), 15019−15042.

https://doi.org/10.1021/acselectrochem.5c00381
ACS Electrochem. 2026, 2, 43−67